Aus der Klinik für Strahlentherapie und Radioonkologie
der Medizinischen Fakultät Mannheim
(Kommissarischer Direktor: PD. Dr. med. Frank Giordano)

Real-Time Ultrasound Image-Guidance and Tracking in External Beam Radiotherapy

Inauguraldissertation
zur Erlangung des Doctor scientiarum humanarum (Dr.sc.hum.)
der Medizinischen Fakultät Mannheim
der Ruprecht-Karls-Universität
zu
Heidelberg

vorgelegt von
Dwi Seno Kuncoro Sihono

aus
Bandung, Indonesia
2019

Dekan: Prof. Dr. med. Sergij Goerdt
Referent: Prof. Dr. Frederik Wenz

TABLE OF CONTENTS

Page

ABBREVIATION LIST

3D	Three Dimensional
4D	Four Dimensional
ABC	Active Breathing Coordinator
AFC	Automatic Fusion and Contour
AP	Anterior-Posterior
ASPK	Autoscan Probe Kit
BED	Biological Effective Dose
BH	Breath-Hold
CBCT	Cone-Beam CT
CT	Computed Tomography
CTV	Clinical Target Volume
CRC	Colorectal cancer
DIBH	Deep Inspiration Breath-Hold
EBRT	External Beam Radiotherapy
HV	Healthy Volunteer
IGRT	Image Guided Radiation Therapy
IMRT	Intensity Modulated Radiation Therapy
kV	kilo-voltage
Linac	Linier Accelerator
LR	Left-Right
MLC	Multi-leaf Collimators
MRI	Magnetic Resonance Imaging
MU	Monitor Units
MV	Megavoltage
NTCP	Normal Tissue Complication Probability
OAR	Organ at Risk
PCC	Pearson correlation coefficient
PTV	Planning Target Volume
RILD	Radiation-induced Liver Disease
RMS	Root Mean Square
RT	Radiation therapy
SBRT	Stereotactic body radiation therapy

SD	Standard Deviation
SI	Superior-Inferior
SS	Step and Shoot
SW	Sliding Window
TAUS	Transabdominal ultrasound
TCP	Tumor Control Probability
TPUS	Transperineal ultrasound
US	Ultrasound
VMAT	Volumetric Modulated Arc Therapy

1 INTRODUCTION

Radiation therapy (RT), or radiotherapy, involves the use of ionizing radiation to cure or relieve the symptoms of cancer. Radiation can often be an alternative primary treatment for many tumor entities and may be offered as non-invasive treatment In addition, a radiotherapy treatment is very often part of a multi modal treatment regimen and besides surgery and chemotherapy an important column in cancer treatment, termed (neo-)adjuvant radiation therapy.

The goal of RT is to deliver a lethal dose of radiation to a well-defined tumor volume while minimizing the dose, and hence damage, to surrounding healthy tissue. Typically, the prescribed radiation dose is divided into equal “fractions” that are delivered in regular time intervals (e.g. daily, bi times daily or every other day) over several weeks. This improves the outcome of treatment by allowing healthy cells to repair damages and repopulate between exposures

As radiotherapy has become more conformal through the development of three-dimensional (3D) planning and delivery techniques such as intensity-modulated radiotherapy (IMRT) and volumetric modulated arc therapy (VMAT), the ability to verify that the planned dose is delivered to the target volume is essential.

Image Guided Radiation Therapy (IGRT) is the use of in-room imaging to adjust for target motion or positional uncertainty (interfraction and intrafraction), and potentially, to adapt treatment to tumor response.[1] The various technologies used for IGRT include 3D ultrasound (3D US),[2] beacon responders, [3] kV/MV cone- or fan-beam CT based methods[4] and Magnetic Resonance Imaging (MRI).[5-7] IGRT has the capability to detect the exact tumor area adjust to organ motion immediately before and/or during treatment. As a result, the Planning Target Volume (PTV) margins can be minimized, leading to a substantial reduction of the target volume to which the radiation dose is prescribed.[8]

IMRT has become the standard radiotherapy technology used for the treatment of prostate cancer, because it allows the delivery of highly conformal radiation dose distributions. IGRT is an essential companion to IMRT that account for daily target anatomy changes and positioning.[9] One commercial solution to monitor intrafraction prostate motion based on ultrasound is the Clarity system (Elekta, Sweden). The Clarity 4D-ultrasound system provides an autoscan probe that provides an

automated ultrasound scanning at the prostate cancer patient's perineum during the treatment. This system is an ideal radiation free modality for real-time imaging.

Although 3D-US has several advantages compared with other modalities, some limitations need to be considered. First is the accuracy of US localization. Some studies established the accuracy of 3D-US to be within 5 mm as compared to CT localization.[10, 11] Accurate spatial reconstruction relies on the accuracy and constancy of the speed of sound within the media. Furthermore, tissue heterogeneity, probe pressure cause deformation and US artifacts[12] have an influence on US imaging based accuracy.

For real time tissue displacement monitoring, there are some issues regarding US performance, including: (1) lack of means to reliably obtain US images remotely over extended periods; (2) slow processing times for quantitative interpretation of US data; and (3) lack of in vivo performance evaluation of the complete US image guidance process.[13]

Current treatment sites where the Clarity system can be used for interfractional and intrafractional image guidance are prostate, uterus, and bladder. Routinely transabdominal ultrasound (TAUS) has been used for pre-treatment interfraction corrections of the prostate. The bladder of the patient should have a constant filling (more than half full) during the treatment course in order to have good image quality and positioning accuracy using this probe. This can be a challenge for patients with genitourinary problems. Transperineal ultrasound (TPUS) has the benefit to solve this problem. Initial studies have reported the prostate imaging performance with good image quality of TPUS.[14-16] Equipped with a motorized probe and automated ultrasound scanning possibility, TPUS can also perform intrafractional real-time monitoring of prostate motion.

Intrafraction motion of prostate can be significant for some patients.[17] Accurate identification of prostate movement can help to determine the ideal margins that can optimize the tumor control probability (TCP) and reduce the normal tissue complication probability (NTCP) at the same time. However, because of the irregular and unpredictable motion of the prostate motion over time, fixed margins may be not sufficient to compensate for this motion.[18] Intrafraction motion compensation and online monitoring methods might be more beneficial.

The feasibility of using the Clarity system for the monitoring of other organs is currently being evaluated. The Clarity system that it is used for this purpose in the

department of radiation oncology and radiotherapy of the university hospital Mannheim is a special research version named “Anticosti”. The Anticosti version is completely new and not commercially available in clinical routine yet. Currently in this department, flattening-filter-free hypofractionated Stereotactic Body Radiotherapy (SBRT) of liver metastases is performed in computer-controlled DIBH and image-guidance with breath-hold cone-beam CT.[19] The feasibility of using computer controlled deep inspiratory breath-hold (DIBH) performed e.g. with the Active Breathing Coordinator (ABC) system to temporarily immobilize the patient’s breathing has been investigated by many authors before.[20-22] The treatment workflow including simulation, planning and treatment delivery is performed at the same DIBH conditions with only minimal margins needed for breathing motion uncertainty. Moderate DIBH results in a reproducible internal organ contour and placement. Liver SBRT using DIBH has been reported as an effective way to reduce liver target motion.[23] However, intra breath-hold motion potentially enlarging the CTV-PTV margin still has to be considered. For intra breath-hold monitoring of the target, the Clarity (Anticosti) system was evaluated.

The purpose of this thesis is to evaluate the efficacy of a Clarity system as an ultrasound based imaging modality for IGRT. For this purpose, measurements, data collection and data analysis with the Clarity system were performed.

- To evaluate the accuracy of Clarity (clinical version) system, some measurements were performed using US phantom in different probe positions and all available US probes.
- To evaluate the intrafractional motion of the prostate, US monitoring data of routinely treated patients with prostate cancer were collected and analyzed.
- To evaluate the accuracy of Clarity (Anticosti) system for upper abdominal target monitoring, some measurements were performed by using a 3D phantom and US phantom programmed with sinusoidal and breathing movement patterns to simulate computer-controlled based breath-hold phases interspersed with spontaneous breathing.
- To evaluate the clinical applicability of the Clarity (Anticosti) system for upper abdominal target monitoring, some measurements were performed in healthy volunteers. The tracking results of healthy volunteers were compared to point surface marker.
- To evaluate the intrafractional motion during breath-hold in liver treatment cases,

US monitoring data of routinely treated patients were collected and analyzed.

1.1 Radiotherapy

Radiotherapy is one of the major modalities in cancer treatment, in addition to surgery and chemotherapy. The main principle in radiotherapy is that the dose in the target volume should be as high as possible, while keeping the dose in healthy tissue as small as possible. The developments of radiotherapy techniques refer to these main principles. These will provide radiotherapy treatment more effective and efficient. The most recent techniques in radiotherapy are IMRT (Intensity Modulated Radiotherapy) including VMAT (Volumetric Modulated Arc Therapy) using IGRT (Image Guided Radiotherapy).

1.1.1 Intensity Modulated Radiation Therapy (IMRT)

Intensity modulated radiation therapy (IMRT) is an advanced technology for radiotherapy treatment that precisely delivers a good dose distribution in the target using photon beams with a steep dose gradient to the healthy tissue surrounding the tumor area.[24, 25] IMRT techniques employ variable intensities from multiple radiation beams that construct highly conformal dose distributions.[26] Each radiation beam is subdivided into hundreds of smaller radiation beamlets with different individual intensities. [27]

There are three types of IMRT that can be delivered using a conventional linac. Those are: Step-and-shoot, sliding window, and volumetric modulated arc therapy (VMAT).[24] These different types of IMRT differ in how the segments are formed by multi-leaf collimators (MLC). MLCs produce irregularly shaped radiation fields.[28] In step-and-shoot IMRT, a dose is delivered using several MLC segments only when the MLC and the gantry are not moving. During beam off time MLC and or the gantry moves to produce the next segment. Sliding-window IMRT uses a dynamic modulating MLC that changes the beam shape and intensity during beam on time with variable dose rate but static gantry beams. VMAT is a fully variable type of IMRT with dynamic modulated MLC, variable dose rates during rotational gantry movement. VMAT can offer faster beam delivery times and more conformal dose distributions.[24, 26]

A standard IMRT plan often uses several fixed angle radiation beams, with the consequence of increasing treatment time. This can affect the intrafractional motion

of the treatment area and the reproducibility of the treatment position. Increased treatment time also could have radiobiological impact due to the possibility of increased tumor cell repair and repopulation.[26, 29, 30]

IMRT plans use larger number of monitor units (MU) compared to conventional (3D) radiotherapy plans. This causes an increase in the low dose radiation amount in the patients' body. The number of MU used in IMRT depends on the IMRT technique. More MU are required in dynamic IMRT techniques, in which each radiation beam is modulated by continuously moving MLCs. [26, 31] The increase in MU and increase in low dose radiation has led to concerns of increased risk of secondary radiation-induced malignancies. [26, 32]

There has been some interest in arc-based therapies to overcome the limitations with fixed gantry field IMRT.[33] VMAT has the capability to deliver a high conformal dose distribution combined with a short treatment time and MU reduction.[26, 34]

1.1.2 Image Guided Radiation Therapy (IGRT)

IMRT is associated with a steep decline in dose outside the target. Because of that, it needs stringent requirements for control of geometric uncertainties (such as setup error, organ motion and tissue deformation). Raised awareness of geometric uncertainties and interfraction variability in tumor position emphasizes the need for image guidance in conjunction with IMRT. When geometric uncertainties such as setup error and organ motion are considered, the dose delivered to the tumor might be substantially lower, whereas that administered to healthy tissues might be higher, than initially planned. [35, 36]

Geometric uncertainties such as setup error, organ motion, and tissue deformation are controlled using target localization systems. Setup errors arise from inconsistencies in the patient's treatment position. Organ motion is related to physiological processes such as breathing motion which can lead to shifts in organ and target position.[37] As the patient progresses through the treatment, target and normal tissue response can lead to volume changes and deformation. As a result, the relative position, size, or shape of the tumor as well as the normal tissues can deviate from the organ models defined in the planning phase of the process.

Several technologies are available to reestablish the patient setup with respect to the machine isocenter prior to each fraction, and to monitor the patient's position

during treatment delivery such as 3D ultrasound (3D US),[2] beacon responders,[3] kV/MV cone- or fan-beam CT based methods[4] and MRI.[5-7]

Decades of development of localization technology using high-energy X-ray beam have led to the current generation of electronic portal imaging devices (EPIDs). While MV EPID technologies have achieved a presence in commercial treatment systems, some factors have prevented the widespread adoption of frequent portal imaging in clinical practice, such as the inherently low contrast of images made by MV energies and field of view limitation.[37] Because of the more pronounced photoelectric absorption in the lower energy range, radiographic imaging with kilovoltage (kV) X-rays offers higher contrast than MV imaging. This translates into greater visibility of bones or implanted markers at a lower imaging dose. Volumetric imaging on a conventional medical linear accelerator can be produced using cone beam CT systems. In a single gantry rotation linier accelerator, volumetric images are reconstructed by back-projection of hundreds of two-dimensional images acquired from a large-area amorphous silicon detector.[37] The picture of a linear accelerator equipped with EPID and cone beam CT can be seen in Figure 1.

Figure 1. The linear accelerator equipped with EPID and cone beam CT.

A number of studies have demonstrated a lack of correlation between prostate position and the localization of pelvic bony anatomy, and the ability to improve target localization using implanted markers as a surrogate.[38-40] The practice of using radiographic markers may not be restricted to passive seeds or wires. Some innovative emerging technologies include a solid-state radiation dosimeter hermetically sealed in a glass tube.[41] The marker includes a mosfet dosimeter, which integrates radiation exposure, and is visible on radiographs and on CT images.

However, the benefits of implanting any form of marker for guidance should be weighed against the risk of infection or tumor seeding along the needle track.

Criteria for the ideal IGRT solution are integrated with RT, high precision, good resolution, soft-tissue contrast, non-invasive, real-time imaging, during treatment, not too expensive and time consuming, and no or little extra radiation dose. IGRT using cone beam CT is associated with increased radiation exposure to the patient. US has the advantages that it does not result in excess radiation exposure, has the capability to show soft tissue, potential tracking, perfusion, Doppler, etc. It also has limits in imaging of bone, lung, and also pressure influence of the detector.[42]

1.1.3 Stereotactic Body Radiation Therapy (SBRT)

Stereotactic body radiation therapy (SBRT), also known as stereotactic ablative radiotherapy (SABR), is a method of external beam radiotherapy (EBRT) that accurately delivers a high dose of irradiation in one or few treatment fractions to an extra cranial target.[43] SBRT is a highly focused radiation treatment that delivers an intensive dose of radiation on a tumor, while restricting the dose to the surrounding healthy tissues. It is a treatment for many patients with limited volume tumors in which surgery may not be an optimal treatment. The major difference of SBRT compared to conventional radiotherapy is the delivery of large doses in a few fractions, which results in a high biological effective dose BED. The practice of SBRT requires a high level of confidence in the accuracy of the entire treatment delivery process.[44, 45] In SBRT, confidence in this accuracy is the result of integration of modern imaging, simulation, treatment planning, and delivery technologies.[45, 46]

1.1.4 Prostate Cancer

Prostate cancer is the second largest incident of cancer in the world.[47] In 2015, prostate cancer was the cancer with the highest incidence for men in 103 countries, and the leading cause of cancer deaths for men in 29 countries.[47] Radiotherapy is one of the primary modalities for treating cancer of the prostate.[48] The most common radiotherapy technique for treating prostatic cancer is EBRT, now often delivered conformally using advanced techniques such as volumetric modulated arc therapy (VMAT) and intensity modulated radiation therapy (IMRT), to spare as much healthy tissue as possible.[49]

There is a strong push towards hypofractionated radiotherapy as a new standard of treatment for external-beam radiotherapy of localized prostate cancer [50-52]. This could potentially cause longer treatment times, lower fraction numbers, higher dose per fraction. Thus real time monitoring for prostate treatments becomes very important for hypofractionated treatment strategies, especially if no high dose rate flattening filter free techniques are used to compensate the longer treatment times. It will allow suitable reactions such as treatment beam interruption or online adaptation if the position deviation of the prostate is larger than a certain pre-defined threshold.[18]

1.1.5 Liver Cancer

The liver can be affected by primary liver cancer, which arises in the liver, or by cancer that forms in other parts of the body and then spreads to the liver. Most liver cancer is secondary or metastatic, meaning it started elsewhere in the body. Colorectal cancer (CRC) is one of the tumors that most often presents with solitary or oligometastasic disease, commonly in the liver.[53] The low tolerance of liver tissue to irradiation raises the risk of the radiation-induced liver disease (RILD). Safe radiation treatment of liver metastases should be possible with a technique that delivers a very conformal radiation dose to the tumor and a minimal radiation dose to surrounding critical tissues. This technique is known as SBRT.[53] To ensure the delivery accuracy, the target position is checked before or during SBRT treatment, by an integrated image acquisition system (IGRT).[45]

Physiological respiratory motions of the liver

Respiratory motions vary from patient to patient, although breathing itself is almost periodic and therefore relatively predictable. Respiratory patterns in a patient may change from fraction to fraction or even during one fraction, so that for a single patient, a general respiratory pattern cannot be assumed.[54] The intrafractional motion of liver tumors in free breathing was described by Kitamura et al. They found the average amplitude of tumor motion in the 20 patients was 4 ± 4 mm (range 1-12 mm), 5 ± 3 mm (range 2-12 mm) and 9 ± 5 mm (range 2-19 mm) in LR, AP and SI, respectively.[55] Balter et al found that the liver moved on average 17 mm in the SI direction between inspiration and expiration.[56]

1.2 Inter and intrafraction motion

Inter and intrafraction motion during radiation therapy has been a widely researched topic, e.g. for breast cancer [57, 58], prostate cancer [59, 60] and lung cancer.[61] Intrafraction motion results in significant geometric and dosimetric uncertainties in radiation treatment planning and dose delivery.[62]

Interfraction motion is the motion seen between images taken on different treatment fractions/days and has both systematic and random components. Systematic interfraction error is the average variation in treatment position calculated from all treatment verification images across a course of radiation therapy for a particular patient, compared with their planning reference image (simulator image or digitally reconstructed radiograph). Random interfraction error is the variability in patient positioning observed between daily treatment verification images. It can vary each day in direction and magnitude.[58]

Intrafraction motion is the variability seen in multiple images acquired in rapid succession during the delivery of a radiation treatment beam or a single daily fraction. Intrafraction error is considered random, as the variations seen in multiple images acquired during one beam-on period are typically related to factors such as patient movement and internal organ motion during the treatment fraction. Random intrafraction error is the variability averaged across all the images taken on one day and compared with the averaged error of all the fractions where images were obtained [58]. Intrafraction motion can be caused by the respiratory, skeletal muscular, cardiac, and gastrointestinal systems.[63] Intrafraction prostate motion is associated with changes in rectal and bladder content, respiratory motion, and changes in overall patient posture.[64]

Several studies quantify interfraction and intrafraction prostate motion using some methods, like using magnetic resonance imaging (MRI),[65] real-time tracking with implanted electromagnetic transponders,[66] and kilovoltage (kV) and megavoltage (MV) imaging of implanted fiducials.[67, 68] Those methods need special effort of implanted clips, transponders or fiducial markers and give exposure to patient.

2 MATERIAL AND METHODS

2.1 Clarity Autoscan Ultrasound (US) System

The Clarity system (Elekta AB, Stockholm, Sweden) is a commercially available intermodal 4D US IGRT system that uses 2D diagnostic ultrasound (US) integrated with optical position-tracking components. The Clarity system consists of a 4D US station in both the CT-Simulator (Clarity-Sim) and treatment room (Clarity-Guide), as seen in Figure 2. The Clarity system is equipped with Clarity Autoscan probe. Clarity Autoscan probe is 2D probe in housing, with motorized control of the sweeping motion. The probe can make a complete scan with 75º sweep in 0.5 seconds.[69] The system aims at tracking of prostate movements during the therapy session and has special patient positioning devices combined with a transperineal diagnostic ultrasound probe with an infrared-detected tracking tree.

3D reference US data are first acquired after the planning-CT in treatment position in the isocenter using the Clarity-Sim station. The isocenter-related 3D US data are automatically fused with CT data on a Clarity Automatic Fusion and Contour (AFC) Workstation. Because US is performed directly after (but not during) planning CT acquisition, the fusion must be controlled offline to avoid errors due to patient motion between CT and US acquisition. The fusion can be modified manually regarding to the anatomy if errors are detected.

Communication with treatment planning systems is accomplished through DICOM via the Clarity Server. This data allows for the determination and comparison of the absolute position of internal anatomical structures of interest at any time during treatment relative to the reference position of the planning-day. If the isocenter is being moved during the planning procedure, this can be corrected in the Clarity workstation with the shift coordinates.

An optically tracked Couch Position Indicator (CPI) is used for reposition the patient as in the treatment plan. The optical position-tracking components and the US data are calibrated relative to each room's reference coordinate system (as defined by CT and LINAC room lasers) using a US QA phantom. The Clarity software combines calibration data from both rooms to establish a common reference coordinate system.

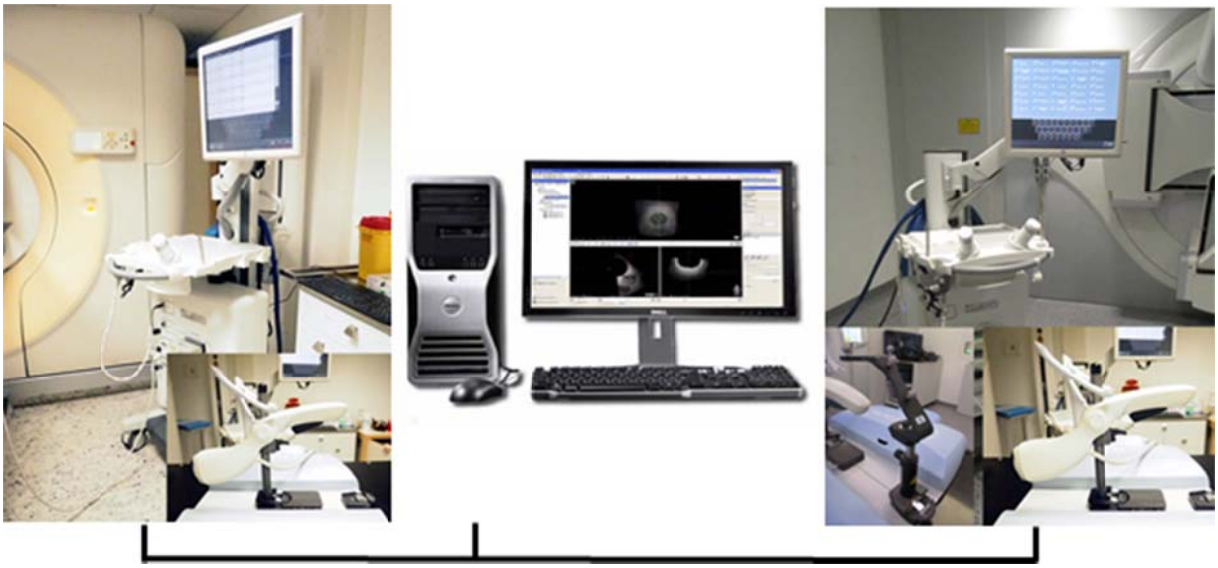

Figure 2. Clarity Autoscan™ (Elekta AB, Stockholm, Sweden) system configuration, Clarity-Sim in Planning-CT room equipped with TPUS Autoscan probe (left) connected via DICOM network to Clarity workstation (server) (middle) and Clarity-Guide in treatment room equipped with TPUS Autoscan probe and Couch Position Indicator (CPI) (right)

System calibration

Precision of measurement is derived from the relationship of the 3D coordinates of the Clarity system and the CT-simulator room or the treatment room. This relationship is established mathematically through a series of calibration procedures. The calibration process determines the transformations (translations and rotations) to convert a given point in the online 3D reconstructed US volume dataset a 2D ultrasound image into 3D coordinates. These coordinates are defined by the room lasers. When calibration/characterization is determined, these transformations are used to construct 3D images using the room coordinate system. The accuracy of the 3D image reconstruction is only as good as the calibration procedure fulfilled the requirement. The calibration/characterization process consists of some steps, these are: phantom calibration, room calibration and probe calibration. The Clarity Tracking System tracks the ultrasound probe in its own coordinate system. Probe calibration determines how the pixels in a 2D ultrasound slice relate to the probe position and orientation. The referencing of the probe position to the room coordinate system is performed after the room calibration. There are four coordinate systems to make relationship between each ultrasound pixel and their corresponding position in room coordinates. Those are the room coordinate system (**R)**, the coordinate system of the tracker (**T)**, the coordinate system of a given 2D ultrasound frame (**F)**, and the probe

coordinate system defined by the definition of the reflective marker array attached to its handle (**P**).[69] A pixel in ultrasound "frame" coordinates $\mathbf{r}_F$ can be transformed to room coordinates $\mathbf{r}_R$ by the equation:

$$\mathbf{r}_R = {}^{R}\mathbf{T}_T \, {}^{T}\mathbf{T}_P \, {}^{P}\mathbf{T}_F \, \mathbf{r}_F \quad (1)$$

where

${}^{P}\mathbf{T}_F$: the 4×4 frame-to-probe transformation matrix

${}^{T}\mathbf{T}_P$: the probe-to-tracker transformation matrix

${}^{R}\mathbf{T}_T$: the tracker-to-room transformation matrix

Room calibration and probe calibration are defined as finding the transformations ${}^{R}\mathbf{T}_T$ and ${}^{P}\mathbf{T}_F$, respectively.[69] The schematic diagram illustrating coordinate transformations for Clarity system calibration can be seen in Figure 3.

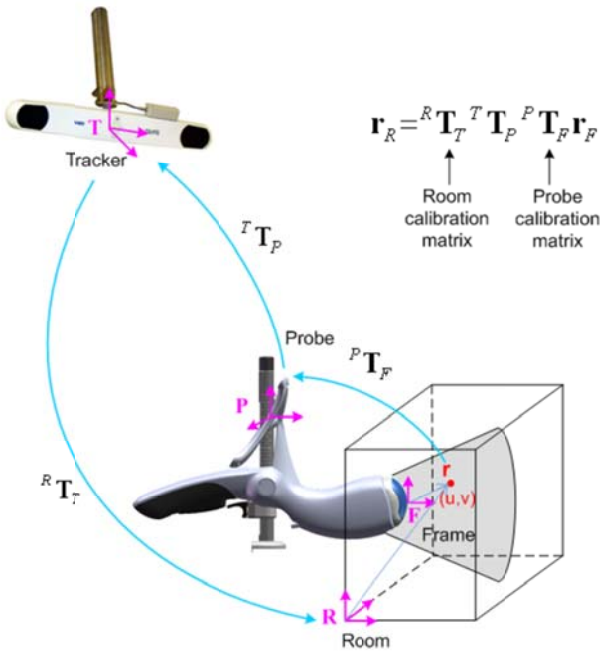

Figure 3. Schematic diagram illustrating coordinate transformations for Clarity system calibration.[69] Image courtesy Elekta AB, Sweden.

The Clarity calibration phantom (CIRS, Norfolk, USA) provides a reliable tool for calibration and quality control procedure of the Clarity system. The phantom is constructed from zerdine, which simulates the acoustical properties of human tissue. The anterior plate consists of a water well with a scanning surface at the bottom, which is transparent to ultrasound when used with appropriate coupling gel or water. The phantom inferior and superior plates also include small embedded ceramic spherical where the phantom coordinate system intersects the plates. The internal

structure of the phantom consists of 2 spheres and 10 rods. It is symmetrical with respect to the sagittal plane. These structures are all anechoic, for easy identification in phantom ultrasound scans. Figure 4 shows a Clarity calibration phantom.

There are two version of Clarity system installed in our department, one is for clinical purpose (currently Clarity software version 4) and the other is for research purpose and commercially not available (codename Anticosti). The Anticosti version is used for upper abdominal lesions target monitoring development and evaluation. Some parameters in this version can be adjusted such as scanning range of the probe, algorithmic options, etc. in order to get optimal settings for a particular tracking situation, in this case the respiratory motion. This system was equipped by the research version of transabdominal 2D probe that has ability of motor-driven sweeping motion. An infrared optical tracking fiducial tree is attached to this probe that can be adjusted for particular probe position. A medical grade fixation arm (CIVCO, USA) was adapted to hold the ultrasound probe (Figure 5). The autoscan transabdominal probe can be seen in Figure 5. The daily quality assurance of the Anticosti system was performed using an ultrasound phantom (Clarity QA phantom, CIRS, Norfolk, USA) with a tolerance of 1 mm in each direction.

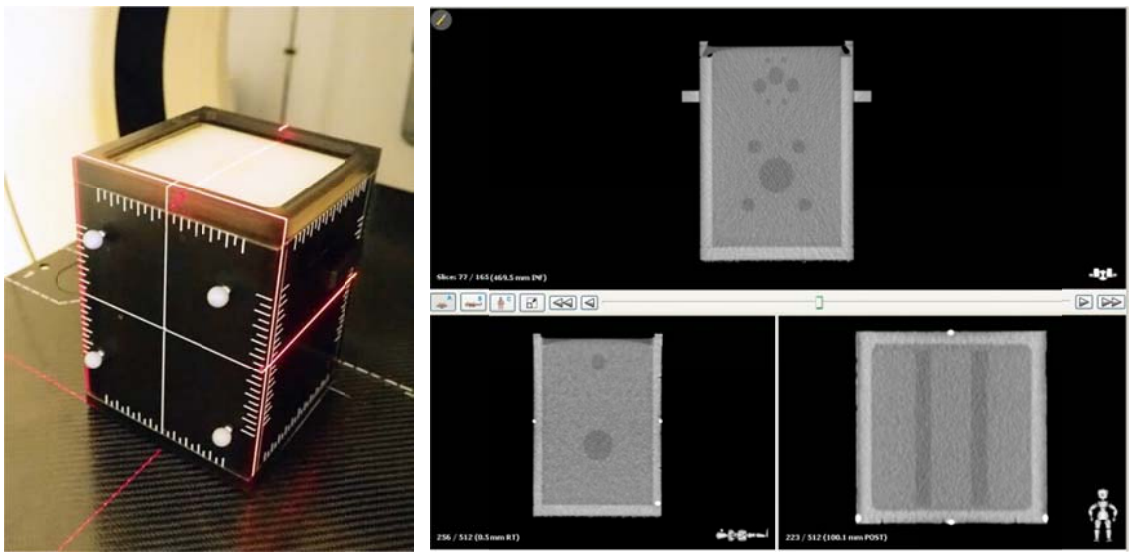

*Figure 4. 3D Clarity QA phantom with infrared markers (*CIRS, Norfolk, USA*) used for calibration (left) positioned to the room lasers and it's CT image in transversal (right above), sagittal (middle) and coronal (right below).*

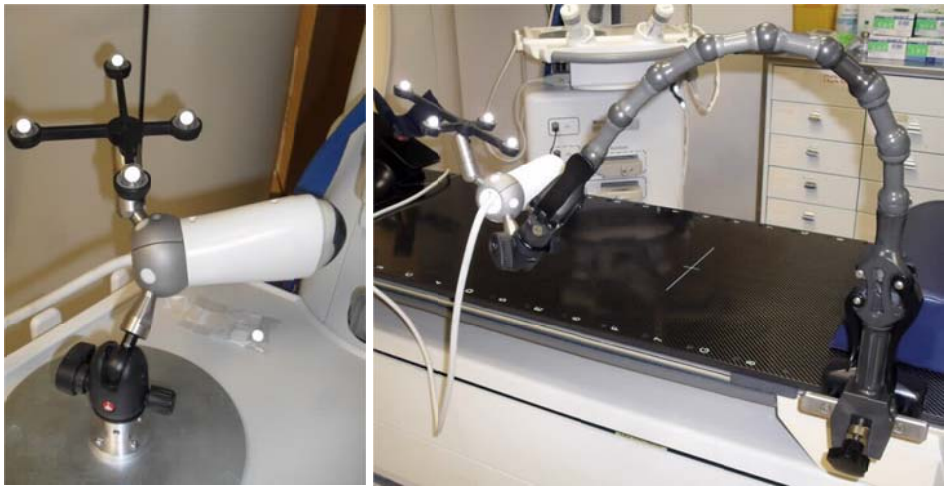

Figure 5. Clarity Autoscan transabdominal probe (left) with fixation arm (CIVCO, USA) (right).

2.2 System Integrity Quality Control

To evaluate the accuracy of Clarity system, the quality control (QC) procedure was performed. The QC procedure is used to verify that the system is properly calibrated prior to use. This ensures that the information provided by the system is as accurate as possible. This QC procedure was adapted to quantify the accuracy of positioning and tracking of Clarity system as well as the implicit registration between CT and US image.

The Clarity QA phantom was scanned with CT and US at the same position (based on room laser) in the CT-simulator room. The US image of the phantom was automatically fused with CT coordinate system in Clarity workstation. The center sphere of the phantom was contoured as the reference target, as well as the reference position for Clarity defined.

The phantom was aligned based on room laser. The phantom was scanned with two different probes: transabdominal ultrasound (TAUS) (Figure 6a) and transperineal ultrasound (TPUS) probe (Figure 6b). Two positions of the phantom were used for TPUS, the vertical (Figure 6b) and the horizontal position (Figure 7). CT and US datasets were implicitly registered in the Clarity workstation. The differences in registration were analyzed for left-right (LR), anterior-posterior (AP), and superior-inferior (SI) directions. The reference positions for positioning and tracking were defined in the Clarity workstation. Several positions/shifts of the phantom were acquired using Clarity-Guide. The differences in positioning and tracking were analyzed for LR, AP, and SI directions.

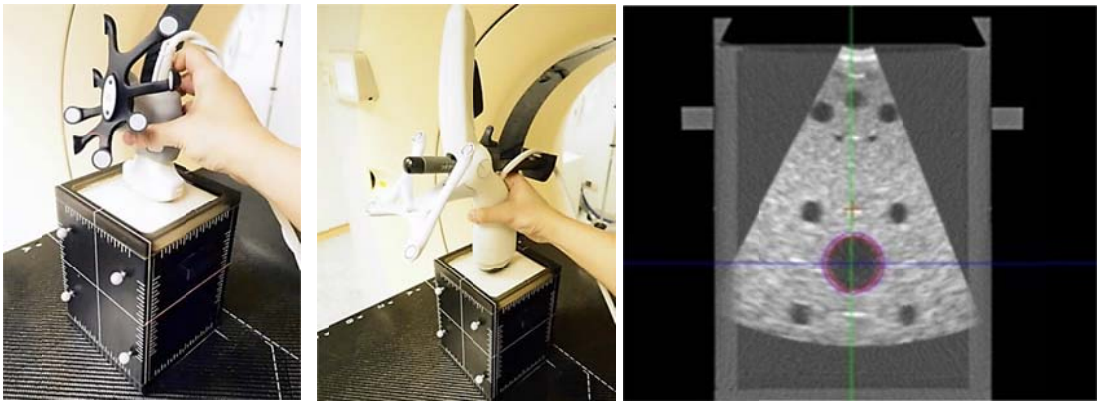

(a) *(b)* *(c)*

Figure 6. Vertical phantom measurement with TAUS (a) and TPUS (b), the contour of sphere inside the phantom as reference target in transverse plane CT (c)

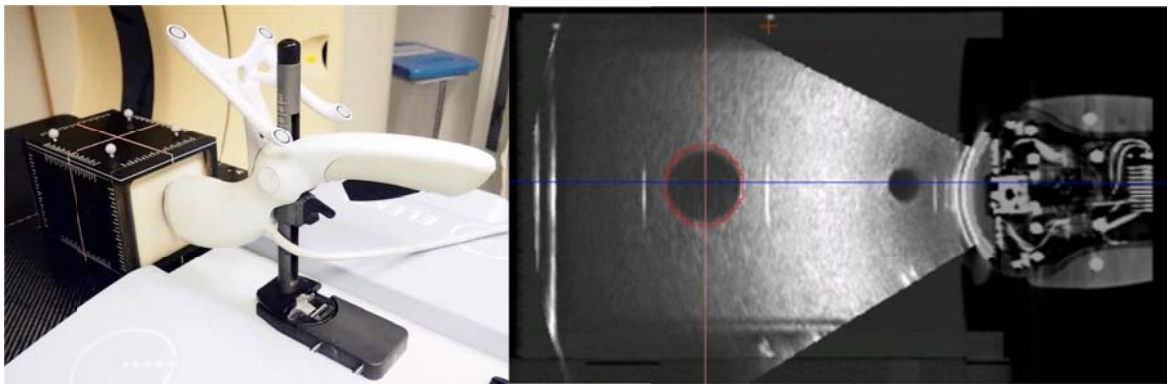

(a) *(b)*

Figure 7. Horizontal phantom measurement with TPUS probe (a) and the contour of sphere inside the phantom as reference target in sagittal plane CT (b).

2.3 Prostate intrafraction motion measurement in patients

This section refers to the published paper Sihono et al. Determination of Intrafraction Prostate Motion During External Beam Radiation Therapy With a Transperineal 4-Dimensional Ultrasound Real-Time Tracking System. International Journal of Radiation Oncology • Biology • Physics, 101: 136-143, 2018 [18]

Patients

38 patients (age 64-87) with prostate cancer (stage, initial PSA, Gleason) were referred for radiotherapy. All patients were treated according to oncologic guidelines with a normofractionated IMRT to the prostate/Seminal vesicles to a cumulative dose of 75Gy. For all patients, daily image guidance has been performed with CBCT

(Elekta etc). Additionally, US-based tracking of the intrafraction motion of the prostate has been performed with Clarity after IRB approval.

Data from 38 patients with primary prostate cancer were prospectively evaluated. The study was approved by the IRB/ethical committee no. 2016-829R-MA. The average age of patients was 74.51±4.50 years (median 75.12 years, range 64–87 years). Patient characteristics can be seen in Table 1.

All patients underwent a reference US scanning after the planning CT scan with the Clarity 4D ultrasound system using autoscan transperineal probe (Figure 1). The planning CT dataset was sent to the treatment planning system (Monaco 5.11, Elekta AB, Stockholm, Sweden); CTVs, PTVs and organs at risk were contoured and a treatment plan was. Afterwards, the CT images, structure set and treatment plan were sent to a record-and-verify system of the Clarity workstation for creating ultrasound IGRT position references.

Patients were treated with an Elekta Versa HD linear accelerator (Elekta AB, Stockholm, Sweden), equipped with 0.5 cm-wide leaves multi-leaf collimator and using energy of 6 or 10 MV with 2 arcs VMAT treatment plans. While interfraction patient positioning was controlled daily by kV cone-beam CT (CBCT), intrafraction motion of the prostate was tracked during 770 fractions by 4D transperineal US.

Each treatment session was analyzed to determine the duration of the time interval in which the prostate was displaced by a certain distance from the optimal reference position. The duration of time the prostate spent at displacements >2, >4, >6, >8, and >10 mm was scored for each direction and also for 3D vector. A total of 770 tracking sessions were available for analysis. The tracking data consisted of the deviation of the geometric center of the prostate from their prescribed position as a function of time. Positive values indicated movement toward the anterior, inferior, and the patient's left direction.

Patient population-based margin calculation

Based on the van Herk formula,[70] the CTV-PTV margin needed to cover the CTV with 95% of the dose for 90% of patients is given by:

$$M = 2.5\,\Sigma + 0.7\sigma \quad (2)$$

where Σ is the standard deviation of the systematic error and σ is the standard deviation of the random error.

Table 1. Prostate patient characteristics data with PTV and prescribed dose (P+SV: Prostate + seminal vesicles)

	Age	Height (cm)	Weight (kg)	PTV and Prescribed Dose
Pat 1	75	170	73	Pelvis 22x2Gy P+SV 8x2Gy Boost P+SV 5x3Gy
Pat 2	72	183	83	Pelvis 22x2Gy P+SV 8x2Gy Boost P+SV 5x3Gy
Pat 3	73	165	71	Pelvis 22x2Gy P+SV 8x2Gy Boost P+SV 5x3Gy
Pat 4	76	178	74	P+SV 30x2Gy Boost P+SV 5x3Gy
Pat 5	75	160	80	P+SV 30x2Gy Boost P+SV 5x3Gy
Pat 6	75	174	98	P+SV 30x2Gy Boost P+SV 5x3Gy
Pat 7	76	162	84	P+SV 30x2Gy Boost P+SV 5x3Gy
Pat 8	68	177	82	P+SV 30x2Gy Boost P+SV 5x3Gy
Pat 9	77	170	75	P+SV 30x2Gy Boost P+SV 5x3Gy
Pat 10	73	173	99	P+SV 30x2Gy Boost P+SV 5x3Gy
Pat 11	72	174	80	P+SV 30x2Gy Boost P+SV 5x3Gy
Pat 12	75	167	74	P+SV 30x2Gy Boost P+SV 5x3Gy
Pat 13	77	176	76	P+SV 30x2Gy Boost P+SV 5x3Gy
Pat 14	73	180	82	P+SV 30x2Gy Boost P+SV 5x3Gy
Pat 15	87	173	74	P+SV 30x2Gy Boost P+SV 5x3Gy
Pat 16	73	179	56	Pelvis 22x2Gy P+SV 8x2Gy Boost P+SV 5x3Gy
Pat 17	70	170	81	P+SV 30x2Gy Boost P+SV 5x3Gy
Pat 18	74	164	76	P+SV 30x2Gy Boost P+SV 5x3Gy
Pat 19	80	174	74	Pelvis 22x2Gy P+SV 8x2Gy Boost P+SV 5x3Gy
Pat 20	70	190	82	P+SV 30x2Gy Boost P+SV 5x3Gy
Pat 21	64	185	85	P+SV 30x2Gy Boost P+SV 5x3Gy
Pat 22	74	182	90	Pelvis 22x2Gy P+SV 8x2Gy Boost P+SV 5x3Gy
Pat 23	75	176	75	P+SV 30x2Gy Boost P+SV 5x3Gy
Pat 24	77	169	77	P+SV 30x2Gy Boost P+SV 5x3Gy
Pat 25	75	181	85	P+SV 30x2Gy Boost P+SV 5x3Gy
Pat 26	75	168	72	P+SV 30x2Gy Boost P+SV 5x3Gy
Pat 27	82	169	73	P+SV 30x2Gy Boost P+SV 5x3Gy
Pat 28	66	173	63	P+SV 30x2Gy Boost P+SV 5x3Gy
Pat 29	75	177	82	P+SV 30x2Gy Boost P+SV 5x3Gy
Pat 30	78	165	72	P+SV 30x2Gy Boost P+SV 5x3Gy
Pat 31	70	175	85	P+SV 30x2Gy Boost P+SV 5x3Gy
Pat 32	73	182	81	Pelvis 22x2Gy P+SV 8x2Gy Boost P+SV 5x3Gy
Pat 33	71	165	80	P+SV 30x2Gy Boost P+SV 5x3Gy
Pat 34	63	174	89	P+SV 30x2Gy Boost P+SV 5x3Gy
Pat 35	75	165	98	Pelvis 22x2Gy P+SV 8x2Gy Boost P+SV 5x3Gy
Pat 36	76	178	86	P+SV 30x2Gy Boost P+SV 5x3Gy
Pat 37	75	163	72	Pelvis 22x2Gy P+SV 8x2Gy Boost P+SV 5x3Gy
Pat 38	78	170	77	P+SV 30x2Gy Boost P+SV 5x3Gy

2.4 Upper abdominal target monitoring – phantom study

This part refers to the publication Sihono et al, A 4D ultrasound real-time tracking system for external beam radiotherapy of upper abdominal lesions under breath-hold. Strahlentherapie und Onkologie, 193: 213-220, 2017 [71]

The Clarity system used for this prospective evaluation is the Anticosti version which is the research version of Clarity after approval of the local IRB No 2014-413M-

MA-§ 23b MPG, amendment 2017. Some parameters in this version can be adjusted such as scanning range of the probe, algorithmic options, etc. in order to get optimal settings for a particular tracking situation, in this case the respiratory motion. This system was equipped by the research version of transabdominal 2D probe that has ability of motor-driven sweeping motion. An infrared optical tracking fiducial tree is attached to this probe that can be adjusted for particular probe position. The autoscan transabdominal probe can be seen in Figure 5.

Clarity Anticosti's monitoring algorithm is based on a prostate tracking model with the assuming spherical shape and slow-moving structure. However, tracking of a faster-moving and non-spherical target as vessel structures in the liver requires setup modifications. For that reason we adjusted the angular scanning range of ultrasound to obtain optimal parameters for tracking along with respiratory motion. The different of angular scanning range image of ultrasound can be seen in Figure 8. The relation between scanning range and sweeping rate can be seen in Table 2. The tracking was carried out with a frame rate of 45 Hz. A medical grade fixation arm (CIVCO, USA) was adapted to hold the ultrasound probe (Figure 5).

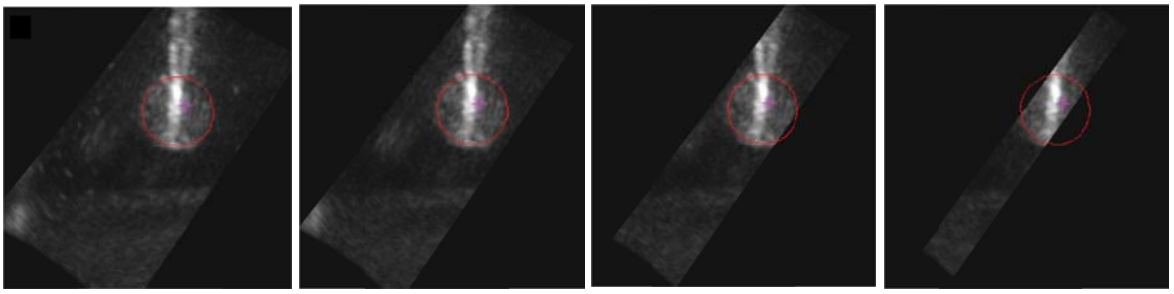

(A) (B) (C) (D)

Figure 8. Sagittal ultrasound image of a spherical structure of the 4D phantom ((Aktina Medical, NY, USA) with different scanning range (A) 40° (B) 30° (C) 20° and (D) 10°.[71]

Table 2. The relation between scanning range and sweeping rate

Scanning range (°)	Sweep rate (Hz)
10	1.4102
20	0.7057
30	0.4706
40	0.3530

To analyze the geometric tracking accuracy of Clarity system along with respiratory motion we performed measurements using US phantom (BAT, Nomos, PA, USA) and respiratory motion platform (CIRS, VA, USA) as well as 4D phantom (Aktina Medical, NY, USA).

US phantom and respiratory motion platform

To access geometric tracking accuracy along with respiratory motion, an US phantom (BAT, Nomos, PA, USA) was secured on a programmable respiratory motion platform (CIRS, VA, USA) (Figure 9).[72] The positioning reference was defined before the measurement. The US phantom was positioned according to the room laser and then scanned by the US. The US image of the US phantom was registered to the CT by the isocenter coordinates in the Clarity AFC Workstation. After the fusion, the central sphere of US phantom was contoured and assigned as tracking target, after that positioning reference defined in the Clarity AFC Workstation. The US image of US phantom can be seen in Figure 9.

The motion platform was programmed to perform repeated mechanical movement to simulate sinusoidal pattern, assumed as respiratory pattern, in 5 mm and 10 mm (Figure 10) amplitudes and several cycle times between 15 s and 60 s.

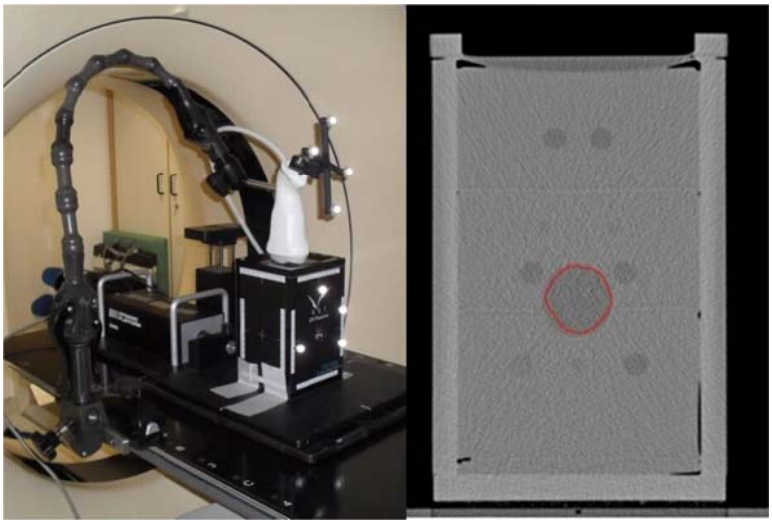

Figure 9. *US phantom with motion platform (BAT, Nomos and CIRS)(left) and the center spherical as tracked target in transverse plane CT (right).*

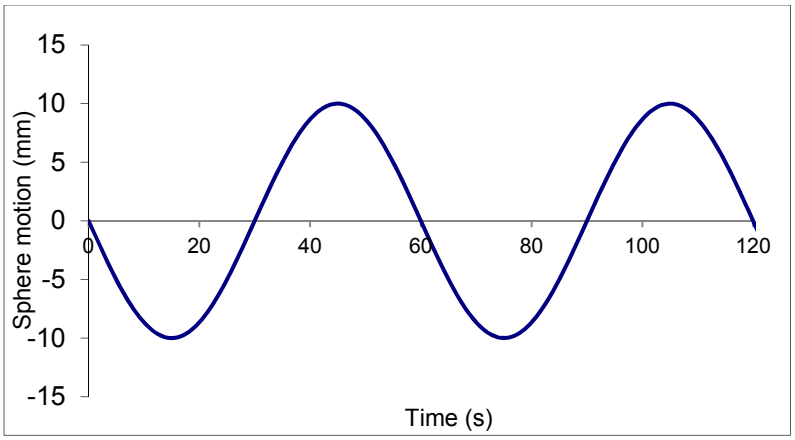

Figure 10. Sinusoidal pattern with amplitude 10 mm and 60 s cycle time.

The motion platform moved in Left-Right (LR) and Superior-Inferior (SI) direction. The Anterior-Posterior (AP) direction could not be measured due to limitation of the motion platform that cannot hold the US phantom in this direction. An external marker (infrared reflector) on the US phantom was used as reference for the phantom motion and optically tracked by the Clarity system. The difference between US detection and marker position was quantified to analyze the geometric tracking accuracy.

4D phantom

A 4D phantom (Aktina Medical, NY, USA) with a spherical structure moving in liquid (salt solution, 60gr salt/kg water) was used (Figure 11). The distance detection check was performed prior each measurement to validate the concentration of the salty liquid. The positioning reference was defined before the measurement. The 4D phantom was positioned regarding to the room laser, where the center of spherical structure was positioned in the intersection of the room laser and then scanned by the US. The US image of the 4D phantom was registered to CT coordinates in the Clarity AFC Workstation. After the fusion, the central sphere of 4D phantom was contoured and assigned as tracking target, after that positioning reference defined in the Clarity AFC Workstation. The US image of 4D phantom can be seen in Figure 11.

The 4D phantom was programmed with sinusoidal pattern in 10 mm amplitudes and cycle times 5 s and 10 s. The phantom also was programmed with breathing movement patterns to simulate computer-controlled breath-hold phases interspersed with spontaneous breathing. The movements were applied in AP and SI direction. Both directions are mostly affected by breathing motion.[73-75] An external

marker (infrared reflector) was attached to the motion mechanical part of the 4D phantom to obtain the actual movement of the sphere with sub-millimeter accuracy (Root Mean Square (RMS) based on the system specification is 0.35 mm.[76] The external marker was detected by the infrared cameras of the Clarity Anticosti system. The difference between US detection and marker position was quantified to analyze the geometric tracking accuracy.

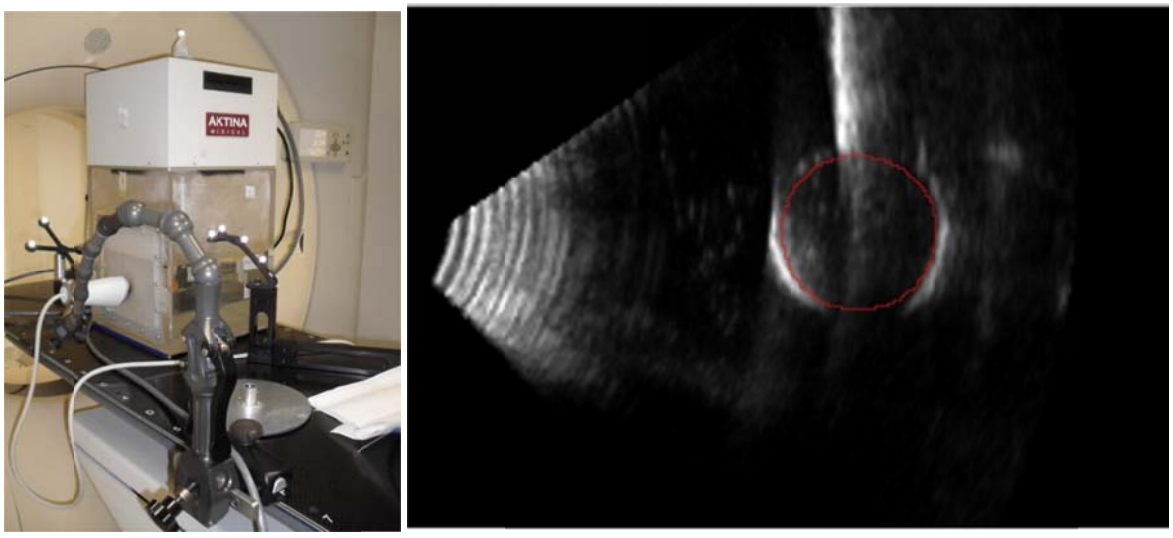

*Figure 11. 4D phantom (*Aktina Medical, NY, USA*) (left) and the center spherical contour as tracked target in transverse plane CT (right).*

2.5 Upper abdominal lesions target monitoring – healthy volunteers

To evaluate the performance of US tracking *in vivo*, 5 healthy volunteers (HV) were set up simulating the clinical situation of repeated DIBH. This study had the permission of the local IRB no 2014-413M-MA-§ 23b MPG. First, upper abdominal US datasets of HV were acquired in computer-controlled breath-hold (ABC, Elekta AB, Sweden) by 2 experienced radiation oncologists. Then the renal pelvis and a portal vein/liver vein were contoured as tracked structure. (Figure 12)

Active Breathing Coordinator (ABC) is a non-invasive device that assists patients maintaining a deep breath during radiotherapy. This device equipped with mouthpiece, hold by patient, attached to a breathing tube. When the patient takes a deep breath, a small valve in the breathing tube closes so no additional air can enter the lungs during the breath-hold.

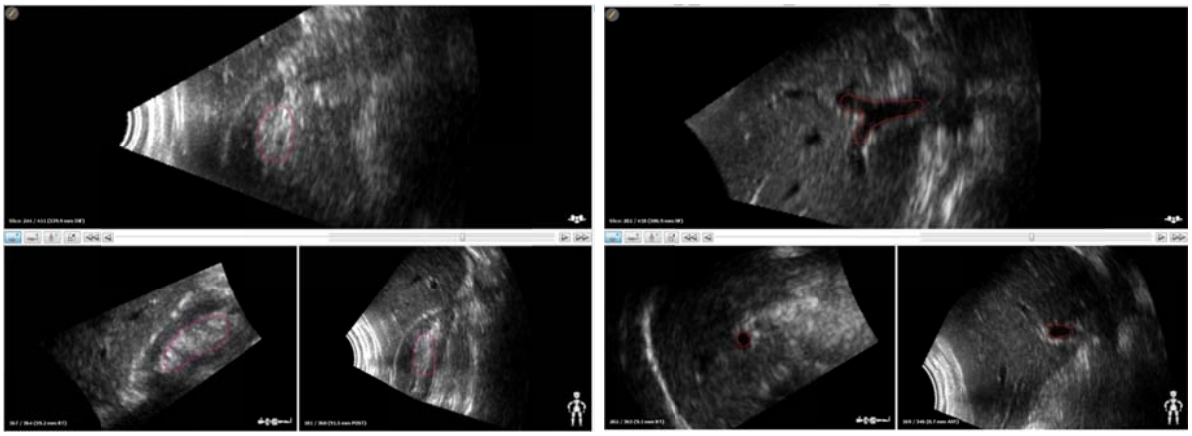

Figure 12. The US image of healthy volunteer with the tracked target of renal pelvis (left) and a portal vein/liver vein (right).

The renal pelvis was as a centroid structure and a portal vein/liver vein was as a non-centroid structure. After the reference position defined in Clarity workstation, the HV was acquired again and monitored by US (breath-hold time 20 s, free breathing phases of 5-6 breath cycles). The scanning range of US was varied (40°, 25° and 10°) to find the optimum performance range of the US. During US monitoring, an external reflective sphere marker placed on the infra-diaphragmatic abdominal wall of the body surface. The infrared camera of Clarity system tracked the reflective sphere marker. The US motion component in SI and AP direction was analyzed offline by comparing with the motion of an external sphere marker. Visual evaluation was performed by experienced radiation oncologist to determine whether the US tracks the correct target. A statistical correlation of surface marker and target motion of good tracking US during individual breath-holds was estimated by the Pearson correlation coefficient (PCC). The PCC is used to verify the US tracking result with the surface marker motion. The setup of US probe on a healthy volunteer can be seen in Figure 13.

2.6 Upper abdominal target monitoring - intrafraction motion in breath-hold in patients treated with SBRT

This part of the thesis is based on the co-authored publication Vogel et al., Intra-breath-hold residual motion of image-guided DIBH liver-SBRT: An estimation by ultrasound-based monitoring correlated with diaphragm position in CBCT. *Radiotherapy and Oncology*, 2018.[77]

Figure 13. US probe setup on healthy volunteer with ABC-based breath-hold and fixation arm.

15 patients (14 men, 1 woman) at different primary tumors (2x hepatocellular carcinoma, 1x melanoma, 1x cholangiocellular carcinoma, 6x colorectal carcinoma, 1x bronchial, 1x oropharyngeal carcinoma, 1x pancreatic cancer, 1x endometrial carcinoma and 1x small cell lung carcinoma) with metastases in the liver, spleen or adrenal gland in the last three years treated at the University Hospital Mannheim (see Table 3) were evaluated. In 2 patients (patient 10 and patient 11), two different metastasis were treated sequentially, so a total of 17 radiotherapy series of were carried out. The average age of the patients is about 64 years with a minimum of 38 and a maximum of 90 years. The prescribed dose was at 9 SBRT series 5x12 Gy, 2 SBRT series 12x5 Gy and the other radiotherapy series each 15x3 Gy, 10x3 Gy, 12x3 Gy, 5x8 Gy, 6x6 Gy or 7x5 Gy. The Ethics Committee agreed to the research project on 20.05.2014 under the letter no 2014-413M-MA-§ 23b MPG.

Table 3. Patient characteristics, HCC = Hepatocellular carcinoma, CA = carcinoma, CRC = colorectal carcinoma*, HNO = HNO-Tumor, CCC = cholangiocellular carcinoma, SCLC = small cell lung cancer.*

	Age	Sex	Weight (kg)	Height (cm)	Tumor Type	Prescribed Dose
Pat 1	82	M	67	173	HCC	15x3 Gy
Pat 2	53	M	76	175	Bronchial-CA	12x5 Gy
Pat 3	90	M	62	161	CRC	10x3 Gy
Pat 4	56	M	70	173	Oropharynx-CA	5x12 Gy
Pat 5	76	M	84	173	HCC	12x3 Gy
Pat 6	84	M	65	165	Melanoma	5x12 Gy
Pat 7	47	M	95	181	CCC	6x6 Gy
Pat 8	55	M	66	176	Pancreas-CA	5x12 Gy
Pat 9	58	M	111	176	CRC	7x5 Gy
Pat 10, PTV1	68	M	72	168	CRC	5x12 Gy
Pat 10, PTV2	68	M	72	168	CRC	5x12 Gy
Pat 11, PTV1	55	F	104	179	Endometrium-CA	5x12 Gy
Pat 11, PTV2	55	F	104	179	Endometrium-CA	5x12 Gy
Pat 12	71	M	103	185	CRC	5x12 Gy
Pat 13	63	M	70	183	SCLC	5x8 Gy
Pat 14	82	M	70	175	CRC	5x12 Gy
Pat 15	74	M	104	178	CRC	12x5 Gy

For radiotherapy planning, each patient received a contrast-assisted, abdominal planning CT (Brilliance Big Bore, Philips, Eindhoven, Netherlands) with a layer thickness of 3 mm and a resolution of 1.2 mm in deep inspiratory breath (DIBH, about 70% of vital capacity) acquired with the ABC system (Elekta AB, Stockholm, Sweden).[72] The reference US image was performed after CT scan using transabdominal Autoscan probe of Clarity Anticosti version in DIBH. As part of the treatment planning, the PTV and the risk organs (liver, central hepatobiliary structures, kidneys, heart, lungs, small intestine, duodenum, stomach, ribs / thoracic wall) were contoured in Monaco 5.11 (Elekta AB, Stockholm, Sweden). The patient's organ structure, plan and CT images exported to Clarity workstation for US to CT image registration. After US to CT image registration, the reference structure (either the GTV itself or a prominent, near-echo-rich surrogate (liver vein, portal vein branch) was set as reference positioning/tracking in Clarity workstation.

During daily positioning of the patient, thoracic and abdominal CBCT was acquired in repeated DIBH (with ABC, 6-7 DIBHs lasting 15-20 s per CBCT). CBCT projections were recorded exclusively during breath-hold. Prior to performing the CBCT, one in five trained professionals (two experienced radiographers, three radiotherapists) acquired the daily US dataset. The additional time required for the construction was documented. The Clarity system tracked the movements of the structure in the liver simultaneously with CBCT and treatment delivery and gave out the position in three planes (SI, AP, and LR) over time.

To assess respiratory excursions, a straymarker was attached to the patient's body surface prior to CBCT. The stray marker consisted of an infrared reflector ball (diameter 11.5 mm) in a plastic bag, which was attached to the same place before each session with an adhesive strip (see Figure 12). The stray marker is not intended for clinical use and was only used to estimate the surface movement. During CBCT and irradiation, the position of the stray marker was detected via infrared cameras of the Clarity system.

SBRT delivery was performed on a flattening filter free linear accelerator (Versa HD, Elekta AB, Stockholm, Sweden) with the ABC breathing control system connected to the linac via a gating interface (Response, Elekta AB, Stockholm, Sweden). Via the gating interface, the radiation beam was only started when the patient was in the breathing curve of the ABC system above a certain threshold. Irradiation was, if possible, performed with the ultrasound probe attached with the scan range of 30°.[71] The ultrasound probe was spared from the primary beam in the treatment plan in these cases.[78] During CBCT and radiation, the position of the target structure could be ultrasonically monitored on a surveillance monitor and the first assumptions made as to whether the device had recognized the structure or not. Within this work, the monitoring ultrasound data acquired during CBCTs and treatment were analyzed.

Each treatment and CBCT sessions was analyzed to determine the fraction of time the target was displaced in breath-hold by a certain distance. The fraction of time the target spent at displacements >2, >4, >6, >8, and >10 mm was scored for each direction and also for 3D. The tracking data consisted of the deviation of the geometric center of the target from their prescribed position as a function of time. Positive values indicated movement toward the anterior, inferior, and the patient’s left direction.

3 RESULTS

3.1 System Integrity Quality Assurance (QA)

To evaluate the accuracy of Clarity system, some measurements of QA procedure were performed using US phantom in different probe positions and all available US probes. The results of the performed QA measurement showed that all phantom and probe combinations (TAUS/TPUS, vertical/horizontal and sim/guide) met the manufacturer's specification criterion. The geometric positioning tolerance for Clarity-Sim and Clarity-Guide is 1 mm according to the manufacturer's specifications. [69] The mean results and standard deviations for the positioning errors are shown in Table 4. The QA has shown an accuracy of maximal 0.5mm in all situations.

Table 4. The accuracy of Clarity system in some probe and phantom configuration. All values are within 1 mm and thus confirming the manufacturer's specifications.

Probe and phantom position	**Clarity (n)**	**LR (mm)** Mean ± SD; median; range	**AP (mm)** Mean ± SD; median; range	**SI (mm)** Mean ± SD; median; range
TAUS – vertical	Clarity-Sim (59)	0.2 ± 0.3; 0.0; -0.8 – 0.7	0.2 ± 0.3; 0.0; -0.1 – 0.0	0.2 ± 0.4; 0.0; -1.0 – 1.0
TPUS – vertical	Clarity-Sim (25)	0.2 ± 0.3; 0.0; 0.0 – 1.0	0.1 ± 0.2; 0.0; -0.5 – 0.0	0.4 ± 0.5; 0.3; 0.0 – 1.0
TPUS – horizontal	Clarity-Sim (21)	0.4 ± 0.5; 0.0; -1.0 – 1.0	0.3 ± 0.5; 0.0; -1.0 – 1.0	0.6 ± 0.4; 1.0; 0.0 – 1.0
TAUS – vertical	Clarity-Guide (39)	0.1 ± 0.1; 0.0; -0.2 – 0.2	0.2 ± 0.2; 0.2; 0.0 – 0.3	0.2 ± 0.1; -0.1; -0.5 – 0.3
TPUS – vertical	Clarity-Guide (42)	0.4 ± 0.3; -0.4; -0.9 – 0.2	0.2 ± 0.1; -0.2; -0.6 – 0	0.3 ± 0.3; -0.1; -1.0 – 0.3
TPUS – horizontal	Clarity-Guide (39)	0.2 ± 0.2; 0.2; -0.3 – 0.5	0.3 ± 0.2; -0.1; -0.7 – 0.6	0.3 ± 0.1; -0.2; -0.7 – 0.2
TPUS – horizontal	Clarity-Guide tracking (400)	0.4 ± 0.3; 0.2; 0.0 – 1.1	0.2 ± 0.1; 0.1; 0.0 – 0.6	0.2 ± 0.1; 0.2; 0.1 – 0.3

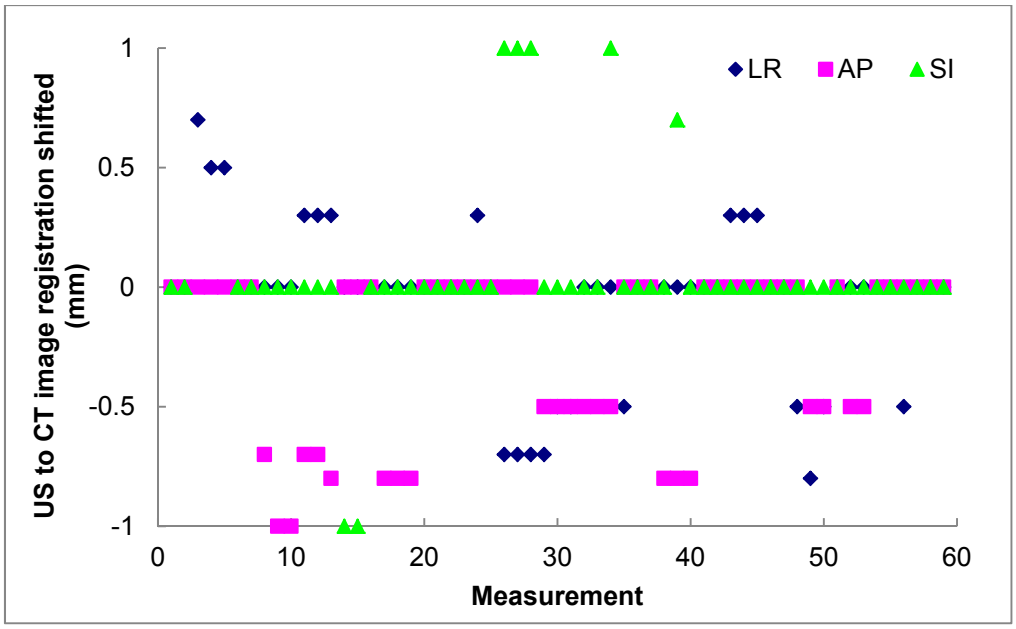

Figure 14. US to CT image registration errors of vertical phantom scanned by TAUS. The results were 0 mm in 63.33%, 61.67% and 81.67% of LR, AP and SI direction, respectively.

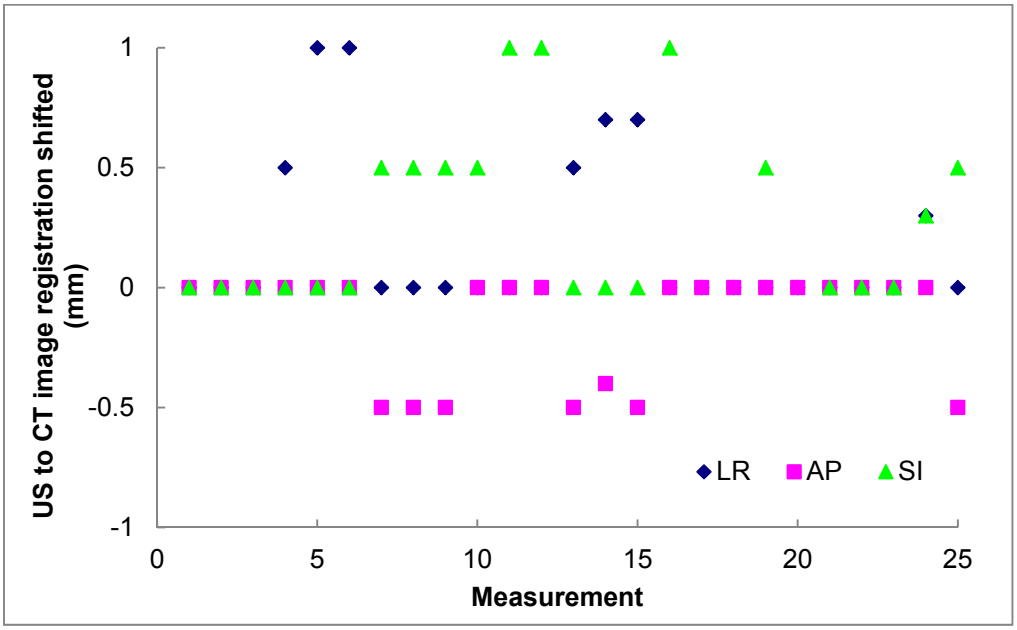

Figure 15. US to CT image registration errors of vertical phantom scanned by TPUS. The results were 0 mm in 69.23%, 69.23% and 46.15% of LR, AP and SI direction, respectively.

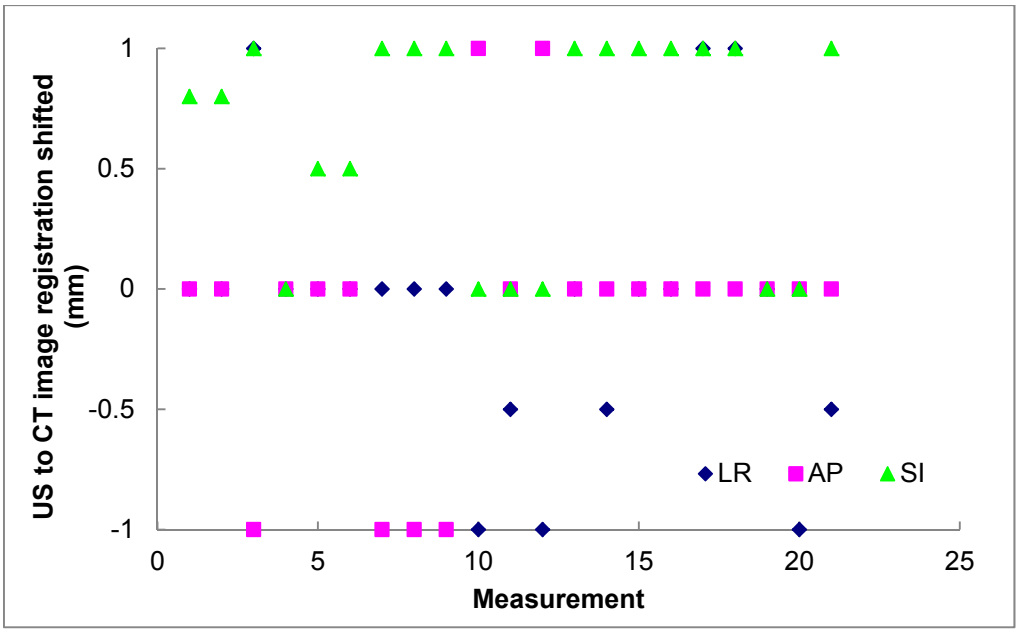

Figure 16. US to CT image registration errors of horizontal phantom scanned by TPUS. The results were 0 mm in 54.55%, 68.18% and 27.27% of LR, AP, and SI direction, respectively.

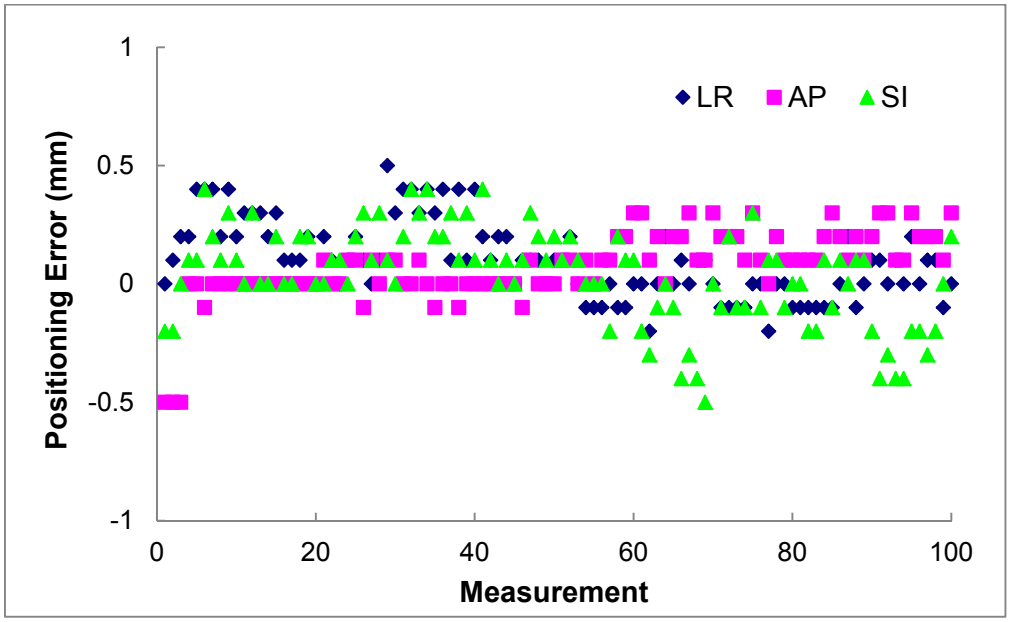

Figure 17. Positioning errors of vertical phantom scanned by TAUS in treatment room. The results were between 0 and 0.5 mm.

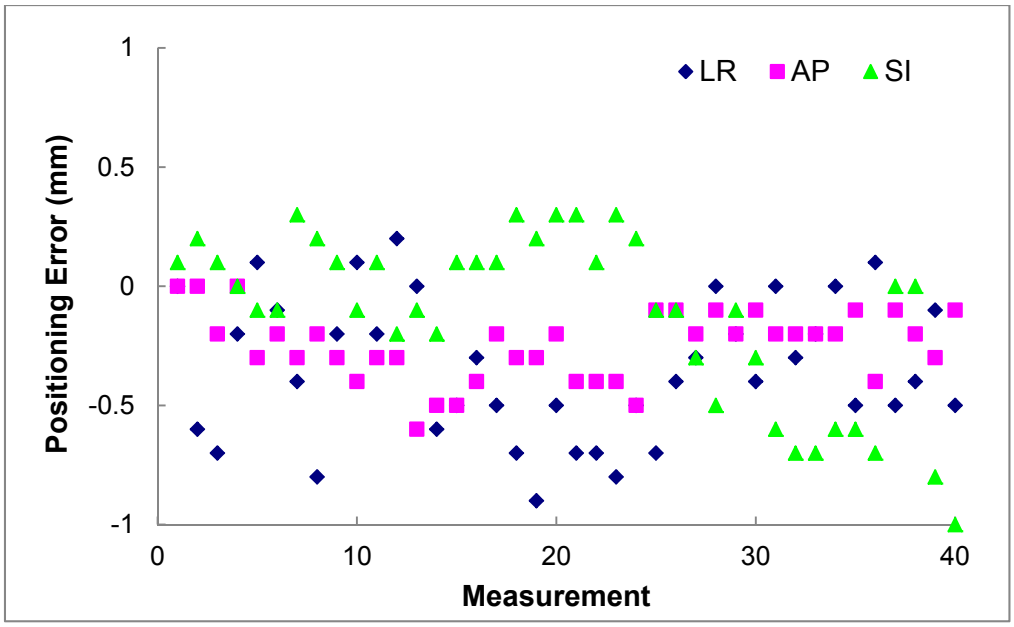

Figure 18. Positioning errors of vertical phantom scanned by TPUS in treatment room. The mean (±SD) results were 0.4 ± 0.3 mm, 0.2 ± 0.1 mm and 0.3 ± 0.3 mm for LR, AP and SI direction, respectively.

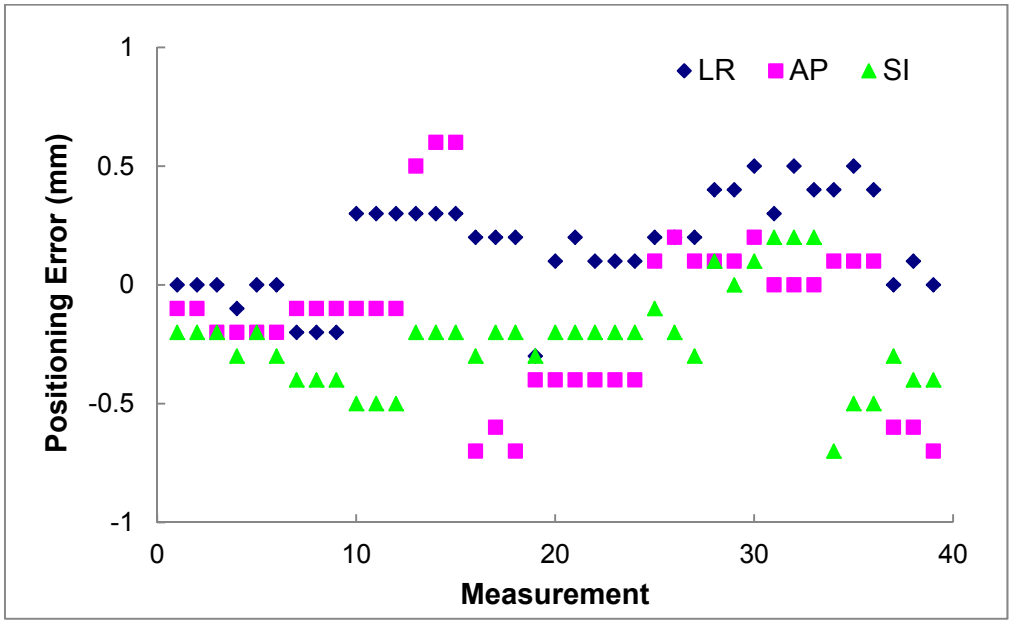

Figure 19. Positioning errors of horizontal phantom scanned by TPUS in treatment room. Most of the results were between 0 and 0.5 mm.

3.2 Prostate intrafraction motion measurement in patients

To evaluate the intrafractional motion of the prostate, US monitoring data of routinely treated patients with prostate cancer were collected and analyzed. All US monitoring sessions were approved by trained radiation oncologists regarding sufficient image quality. 96% of all available monitoring sessions were judged to have a sufficient sonographic image quality and were included to the evaluation. The mean duration (± SD) of each monitoring session was 254s (± 28s) with the range between 210s and 324s.

A wide range of prostate displacements was observed among the 770 fractions. The results can be seen in Figure 20 that shows the histogram of prostate displacement from all fractions in all directions including the 3D vector. Most of prostate displacements were within 2 mm, which is 97.01%, 92.24%, and 95.77% of all monitoring data in LR, AP, and SI direction, respectively.

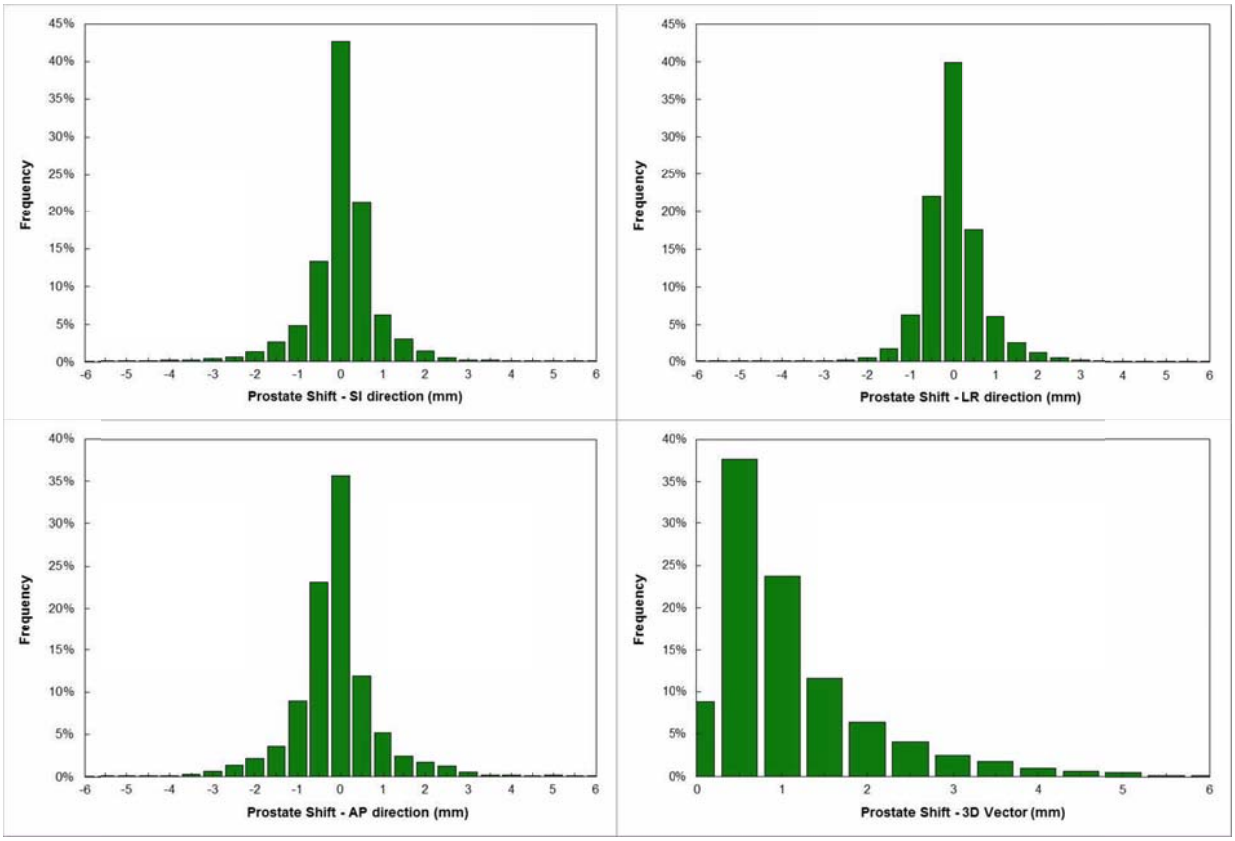

Figure 20. Histogram of prostate intrafraction motion in SI, LR, AP direction and 3D vector. The prostate displacements were within 2 mm, which is 97.01%, 92.24%, and 95.77% of all monitoring data in LR, AP, and SI direction, respectively.

The observed mean, median, and range of percentage data of 3D vector prostate displacements >2, >4, >6, >8, and >10 mm from all 770 fractions are presented in Table 5.

Table 5. Percentage of data the prostate was displaced by >2, >4, >6, >8, and >10 mm from all 770 fractions.

	3D vector > 2 mm	3D vector > 4mm	3D vector > 6 mm	3D vector > 8 mm	3D vector > 10 mm
Mean	12.49%	2.29%	0.56%	0.24%	0.11%
SD	22.39%	9.64%	5.01%	3.10%	1.78%
Median	0.00%	0.00%	0.00%	0.00%	0.00%
Min	0.00%	0.00%	0.00%	0.00%	0.00%
Max	99.37%	86.99%	71.55%	62.83%	41.40%

The largest percentage values for prostate displacements (3D vector) of >2, >4, >6, >8, and >10 mm that occurred in one treatment fraction of a patient were 99.37%, 73.48%, 61.37%, 31.11%, and 21.92% of the fraction data. Analyzing all fractions for this patient, the corresponding values were 27.24%, 9.48%, 3.57%, 1.45%, and 1.02% as it can be seen in Table 6. All individual patient data are presented in Table 6 for the 3D vector displacement as well as prostate volume, number of recorded US sessions and average US tracking time.

The magnitude and duration of the prostate displacements varied widely among the 38 patients. The average, median, and range of values observed for the population of 38 patients for each of the three directions, as well as the 3D vector, are presented in Table 7.

The boxplots of the prostate displacements (3D vector) for each patient are shown in Figure 21. The horizontal band indicates the median, the lower and the upper edges of the box explain the first (25^{th}) and third (75^{th}) quartiles. The lower and the upper extremes of the whiskers, display the 5% and 95% quantiles values. Single data point outliers are the maximum prostate displacements. Table 8 shows the mean ($\pm$ SD) displacement of prostate for each patient in SI, LR, AP and 3D vector.

Table 6. Prostate volume, US session amount, average US tracking time and the percentage of time the prostate was displaced by >2, >4, >6, >8, and >10 mm for each patient.

Pat No.	Prostate Volume (cc)	US Session	Average US Tracking Time (s)	3D Vector Prostate Displacement				
				> 2 mm (%)	> 4 mm (%)	> 6 mm (%)	> 8 mm (%)	> 10 mm (%)
1	62.25	5	321	9.47	0.00	0.00	0.00	0.00
2	74.24	9	324	28.76	5.44	0.00	0.00	0.00
3	34.07	4	229	0.00	0.00	0.00	0.00	0.00
4	51.53	26	260	23.35	3.91	1.28	0.00	0.00
5	49.01	18	264	17.19	3.88	0.22	0.00	0.00
6	35.70	22	282	8.14	0.85	0.00	0.00	0.00
7	20.29	21	281	16.22	0.82	0.07	0.00	0.00
8	57.9	22	297	23.73	4.32	0.00	0.00	0.00
9	30.55	26	309	25.55	0.33	0.00	0.00	0.00
10	45.75	20	279	33.64	6.78	0.86	0.66	0.29
11	57.62	18	260	5.82	0.35	0.06	0.00	0.00
12	65.87	17	245	5.55	1.39	0.00	0.00	0.00
13	70.58	19	267	27.24	9.48	3.57	1.45	1.02
14	52.13	22	239	19.27	1.87	0.00	0.00	0.00
15	29.23	23	232	7.49	0.16	0.00	0.00	0.00
16	33.44	7	220	25.63	2.22	1.03	0.67	0.00
17	22.58	27	237	0.48	0.00	0.00	0.00	0.00
18	70.49	19	210	8.75	1.81	0.21	0.00	0.00
19	117.72	6	253	7.10	0.00	0.00	0.00	0.00
20	42.34	33	247	8.86	2.12	1.21	0.10	0.00
21	40.49	24	221	5.08	0.00	0.00	0.00	0.00
22	83.28	9	248	35.46	2.17	0.00	0.00	0.00
23	32.67	26	275	29.48	16.61	10.79	6.25	5.88
24	53.34	23	240	10.88	2.84	0.00	0.00	0.00
25	38.04	28	239	20.18	5.64	2.30	0.00	0.00
26	82.99	30	259	4.63	0.16	0.00	0.00	0.00
27	51.18	30	212	4.96	1.20	0.04	0.00	0.00
28	65.05	33	226	10.21	0.16	0.00	0.00	0.00
29	19.32	29	232	8.78	3.31	1.70	0.96	0.03
30	42.34	18	252	24.14	7.15	0.05	0.05	0.05
31	135.44	27	271	43.45	11.41	6.69	5.60	1.15
32	22.88	10	273	17.99	1.91	0.00	0.00	0.00
33	52.83	27	243	0.49	0.08	0.04	0.01	0.01
34	57.27	26	245	1.49	0.04	0.01	0.01	0.01
35	69.9	7	236	13.39	0.02	0.00	0.00	0.00
36	58.48	27	248	24.37	6.29	0.01	0.00	0.00
37	37.25	9	271	8.40	1.16	0.00	0.00	0.00
38	48.70	23	222	0.29	0.00	0.00	0.00	0.00

Table 7. Percentage of time the prostate was displaced by >2, >4, >6, >8, and >10 mm calculated from total tracking time for each patient

		> 2 mm (%)	> 4 mm (%)	> 6 mm (%)	> 8 mm (%)	> 10 mm (%)
3D vector						
	Mean	14.89	2.79	0.79	0.41	0.22
	SD	11.21	3.67	2.10	1.35	0.97
	Median	10.55	1.60	0.00	0.00	0.00
	Min	0.00	0.00	0.00	0.00	0.00
	Max	43.45	16.61	10.79	6.25	5.88
AP						
	Mean	7.14	0.98	0.23	0.16	0.15
	SD	6.69	2.02	0.98	0.94	0.94
	Median	4.56	0.04	0.00	0.00	0.00
	Min	0.00	0.00	0.00	0.00	0.00
	Max	26.12	9.77	5.92	5.79	5.78
LR						
	Mean	3.15	0.51	0.22	0.07	0.00
	SD	4.10	1.39	0.95	0.38	0.00
	Median	1.51	0.00	0.00	0.00	0.00
	Min	0.00	0.00	0.00	0.00	0.00
	Max	14.42	7.75	5.66	2.34	0.00
SI						
	Mean	3.68	0.65	0.21	0.16	0.08
	SD	4.46	2.23	1.02	0.95	0.48
	Median	2.85	0.00	0.00	0.00	0.00
	Min	0.00	0.00	0.00	0.00	0.00
	Max	14.91	13.00	6.25	5.84	2.96

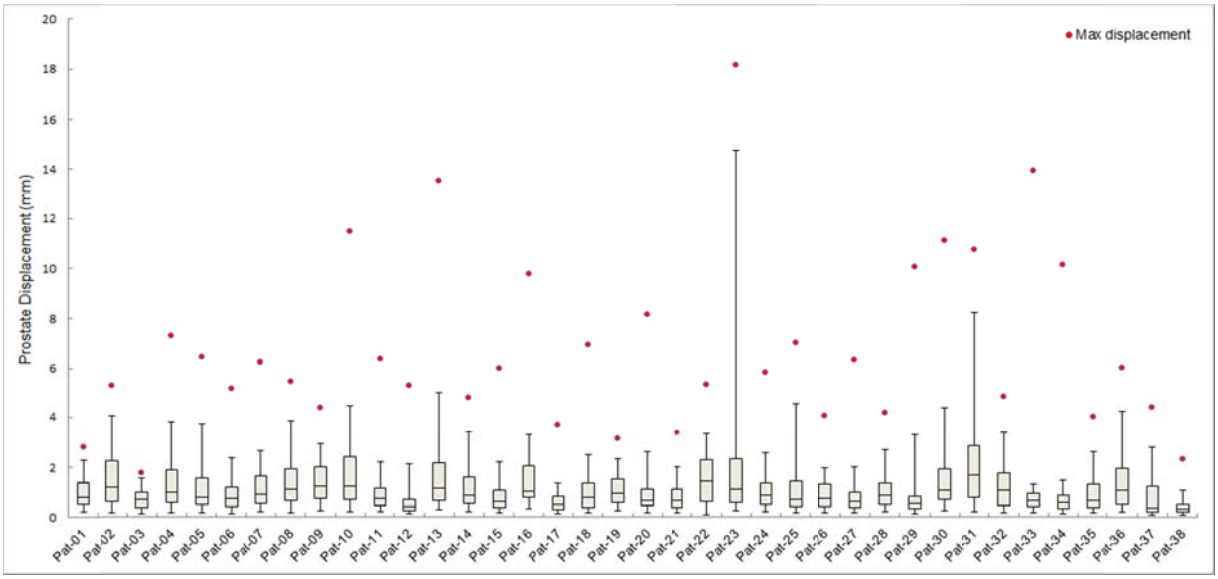

Figure 21. Boxplots of the prostate displacements (3D vector) for each patient. The horizontal band within the box indicates the median, the lower and the upper edges of the box explain the first (25th) and third (75th) quartiles. The lower and the upper extremes of the whiskers, display the 5% and 95% values. Single data point outliers are the maximum prostate displacements.

Table 8. Mean displacement of prostate for each patient in SI, LR, AP and 3D vector

Patient	SI	LR	AP	3D Vector
1	0.29 ± 0.64	0.17 ± 0.27	-0.40 ± 0.62	0.97 ± 0.46
2	-0.15 ± 0.45	-0.05 ± 0.78	0.34 ± 1.12	1.41 ± 0.63
3	0.40 ± 0.33	-0.22 ± 0.24	0.03 ± 0.27	0.73 ± 0.23
4	0.27 ± 0.64	0.28 ± 0.74	-0.34 ± 0.99	1.29 ± 0.95
5	0.07 ± 1.12	-0.18 ± 0.39	-0.03 ± 0.71	1.30 ± 0.94
6	-0.17 ± 0.58	-0.05 ± 0.31	0.01 ± 0.55	0.90 ± 0.47
7	0.38 ± 0.67	-0.10 ± 0.30	-0.33 ± 0.75	1.15 ± 0.59
8	0.27 ± 0.59	0.82 ± 0.42	-0.38 ± 0.67	1.23 ± 0.72
9	0.23 ± 0.75	-0.41 ± 0.40	-0.49 ± 0.80	1.40 ± 0.46
10	-0.43 ± 1.02	-0.17 ± 0.67	0.48 ± 1.15	1.55 ± 1.06
11	0.19 ± 0.37	0.14 ± 0.38	-0.40 ± 0.58	0.92 ± 0.41
12	0.06 ± 0.35	-0.16 ± 0.15	-0.06 ± 0.37	0.56 ± 0.34
13	-0.12 ± 1.02	0.18 ± 1.02	0.26 ± 0.92	1.61 ± 1.47
14	-0.40 ± 0.59	0.37 ± 0.50	0.61 ± 0.80	1.27 ± 0.78
15	0.13 ± 0.51	-0.20 ± 0.27	-0.32 ± 0.51	0.78 ± 0.48
16	-0.37 ± 0.89	-0.62 ± 0.55	0.26 ± 0.55	1.51 ± 0.79
17	0.12 ± 0.24	-0.16 ± 0.33	-0.19 ± 0.27	0.58 ± 0.28
18	0.02 ± 0.45	0.05 ± 0.38	0.15 ± 0.92	1.01 ± 0.63
19	0.07 ± 0.30	0.81 ± 0.40	0.14 ± 0.34	1.05 ± 0.36
20	-0.01 ± 0.33	-0.25 ± 0.69	-0.25 ± 0.70	0.88 ± 0.82
21	0.03 ± 0.46	0.04 ± 0.24	-0.33 ± 0.45	0.75 ± 0.39
22	-0.11 ± 0.40	0.33 ± 1.05	0.28 ± 1.05	1.55 ± 0.91
23	0.47 ± 1.60	-0.02 ± 0.48	-0.44 ± 1.51	1.67 ± 1.80
24	0.12 ± 0.38	0.33 ± 0.52	-0.24 ± 0.56	0.97 ± 0.49
25	-0.05 ± 0.73	-0.19 ± 0.51	0.41 ± 0.81	1.01 ± 0.94
26	0.01 ± 0.35	-0.03 ± 0.46	-0.28 ± 0.44	0.78 ± 0.38
27	0.02 ± 0.44	-0.01 ± 0.36	-0.08 ± 0.58	0.80 ± 0.52
28	-0.32 ± 0.57	-0.22 ± 0.43	0.29 ± 0.59	1.03 ± 0.49
29	-0.01 ± 0.55	0.04 ± 0.72	-0.07 ± 0.55	0.79 ± 0.88
30	0.12 ± 1.02	0.20 ± 0.92	-0.10 ± 0.94	1.53 ± 1.00
31	0.56 ± 0.71	0.23 ± 1.49	-0.92 ± 1.05	1.89 ± 1.33
32	0.38 ± 0.47	-0.40 ± 0.57	-0.66 ± 0.66	1.25 ± 0.56
33	0.07 ± 0.38	0.00 ± 0.34	-0.03 ± 0.43	0.69 ± 0.25
34	0.01 ± 0.45	-0.20 ± 0.30	-0.07 ± 0.41	0.66 ± 0.37
35	-0.13 ± 0.47	0.20 ± 0.72	0.15 ± 0.43	0.98 ± 0.53
36	-0.21 ± 0.56	-0.18 ± 0.58	0.43 ± 0.91	1.29 ± 0.69
37	0.02 ± 0.46	-0.36 ± 0.70	-0.25 ± 0.48	0.73 ± 0.82
38	-0.03 ± 0.29	-0.03 ± 0.15	-0.09 ± 0.16	0.39 ± 0.23

The relation of prostate displacement with time is listed in Figure 22. The percentage of prostate displacement frequency increased with longer observation time. At 60 s, a 3D vector of prostate displacement > 2 mm could be observed in 0.67% of the data. The percentage values increased to 2.42%, 6.14%, and 9.35% at 120 s, 180 s and 240 s, respectively.

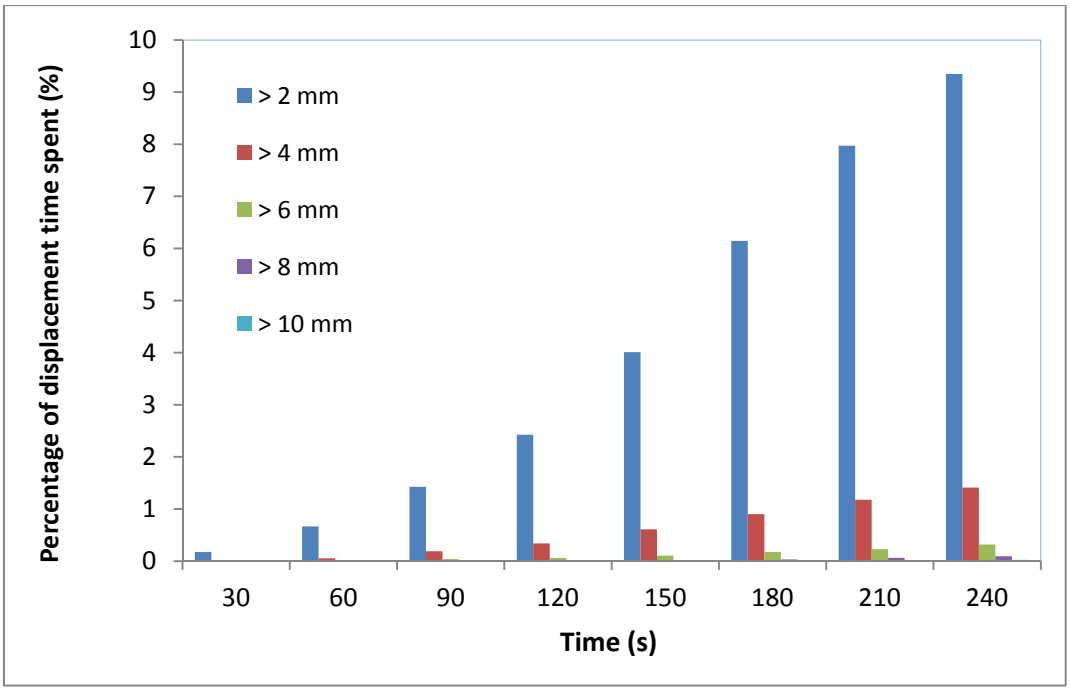

Figure 22. The histogram of prostate displacement (3D vector) related to time from all 770 fractions. The percentage of prostate displacement frequency increased with longer observation time.

The mean (μ), the systematic error (Σ) and the random error (σ) of intrafraction motion of prostate were μ = (0.01, -0.08, 0.05) mm, Σ = (0.30, 0.34, 0.23) mm and σ = (0.59, 0.73, 0.64) mm in LT, AP and SI direction respectively. Using the van Herk formula, a margin between the CTV and PTV was calculated to account for intrafraction motion. Margins of 1.25 mm, 1.33 mm, and 1.10 mm were calculated in the LR, AP, and SI directions, regarding the intrafraction residual motion respectively.

3.3 Upper abdominal target monitoring – phantom study

Ultrasound phantom and motion platform

The first experiment using ultrasound phantom and 4D motion platform was performed with default settings of the US system (40° scanning range) with different cycle times (T) of sinusoidal patterns (amplitude, A=10 mm). The tracking accuracy decreased with decreasing cycle times, as it can be seen in Figure 20. The differences between the measurement and the reference position values (mean standard ± standard deviation) were 0.38 ± 0.32 mm, 0.62 ± 0.46 mm, 1.10 ± 1.10 mm, and 1.71 ± 1.12 mm for 60s, 45s, 30s and 15s, respectively. For a fixed cycle time of 60s and a variation of scanning range, the results were 0.38 ± 0.32 mm, 0.32 ± 0.20 mm, 0.24 ± 0.15 mm, and 0.23 ± 0.15 mm for 40°, 30°, 20° and 10° scanning

range, respectively. The results have the same trend for fixed cycle time of 6s with variation of scanning range in 2 different amplitudes, 5 and 10 mm. The results for amplitude 5 cm were 1.10 ± 1.45 mm, 0.53 ± 0.92 mm, 0.45 ± 0.52 mm, 0.39 ± 0.38 mm for 40°, 30°, 20° and 10° scanning range, respectively. The results for amplitude 5 mm were 2.16 ± 3.02 mm, 1.29 ± 2.55 mm, 1.19 ± 1.15 mm, 0.62 ± 0.74 mm for 40°, 30°, 20° and 10° scanning range, respectively. All results are summarized in Table 9.

4D phantom

The US system could track the sphere motion in the phantom using two sinusoidal pattern (cycle time 5s and 10s, amplitude 10 cm) and five breathing patterns simulating computer-controlled breath-hold phases interspersed with spontaneous breathing, as it can be seen in Figure 24. The accuracy of ultrasound tracking increased with decreasing the scanning range. The differences between the measurement and the reference (mean ± standard deviation) of the sphere motion can be seen in Table 10. Figure 25 shows the measurement result from one representative breathing pattern with different scanning ranges (10°, 20°, 30° and 40°).

Table 9. The differences between the measurement of ultrasound phantom in motion platform and the reference of sinusoidal patterns

Scanning range (°)	Differences between the measurement and the reference of sinusoidal pattern with amplitude A and cycle time T (mean ± standard deviation) in mm		
	A = 10 mm, T = 18s	A = 10 mm, T = 6s	A = 5 mm, T = 6s
10	0.34 ± 0.29	0.62 ± 0.74	0.39 ± 0.38
20	0.78 ± 0.76	1.19 ± 1.15	0.45 ± 0.52
30	0.89 ± 0.66	1.29 ± 2.55	0.53 ± 0.90
40	1.45 ± 1.18	2.16 ± 3.02	1.10 ± 1.45

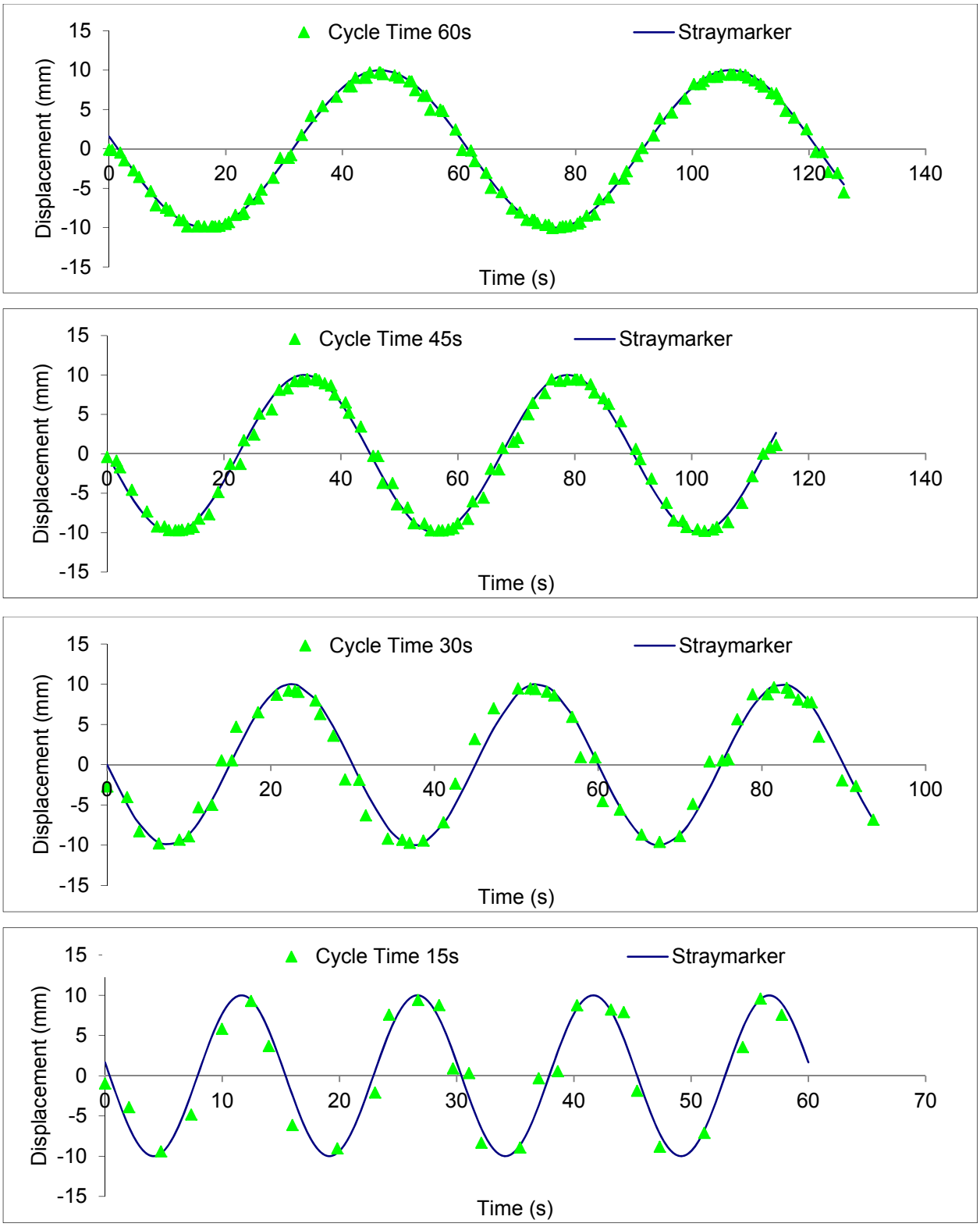

Figure 23. The measurement results using ultrasound phantom and motion platform with different cycle times. The tracking accuracy decreased with decreasing cycle times (faster motion).

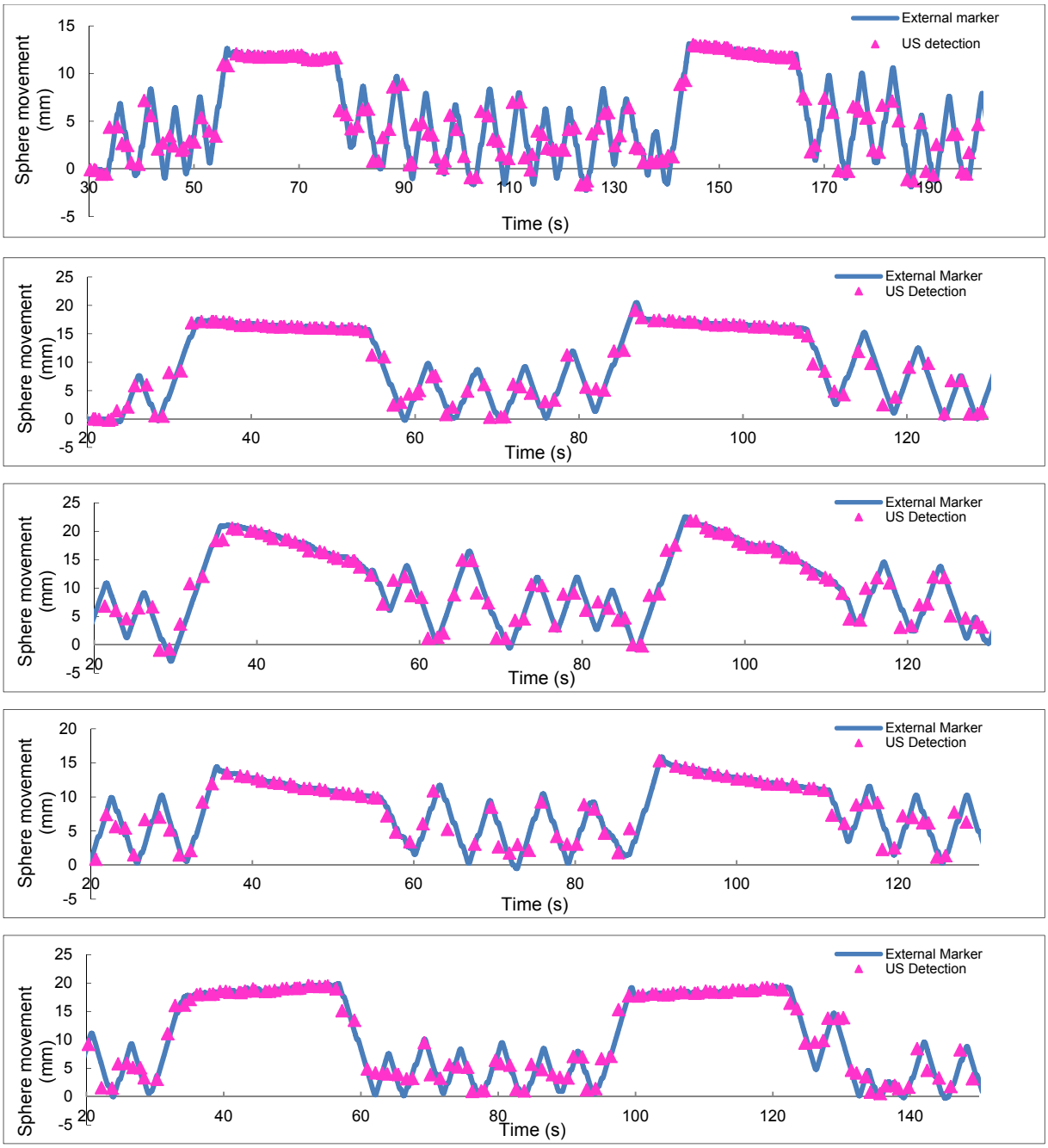

Figure 24. The results of five breathing patterns simulating computer-controlled breath-hold phases interspersed with spontaneous breathing in 30° scanning range.

Table 10. The differences between the measurement and the reference position (mean ± standard deviation) (N=56)) for a target motion with amplitudes of 5 – 20 mm and a cycle time of 5 s.

Scanning range (°)	Differences between the measurement and the reference (mean ± standard deviation) position in mm	
	Sinusoidal pattern	Breathing pattern
10	0.39 ± 0.41	0.47 ± 0.62
20	0.81 ± 0.84	0.56 ± 0.67
30	1.35 ± 1.57	0.97 ± 1.17
40	1.60 ± 1.88	1.13 ± 1.46

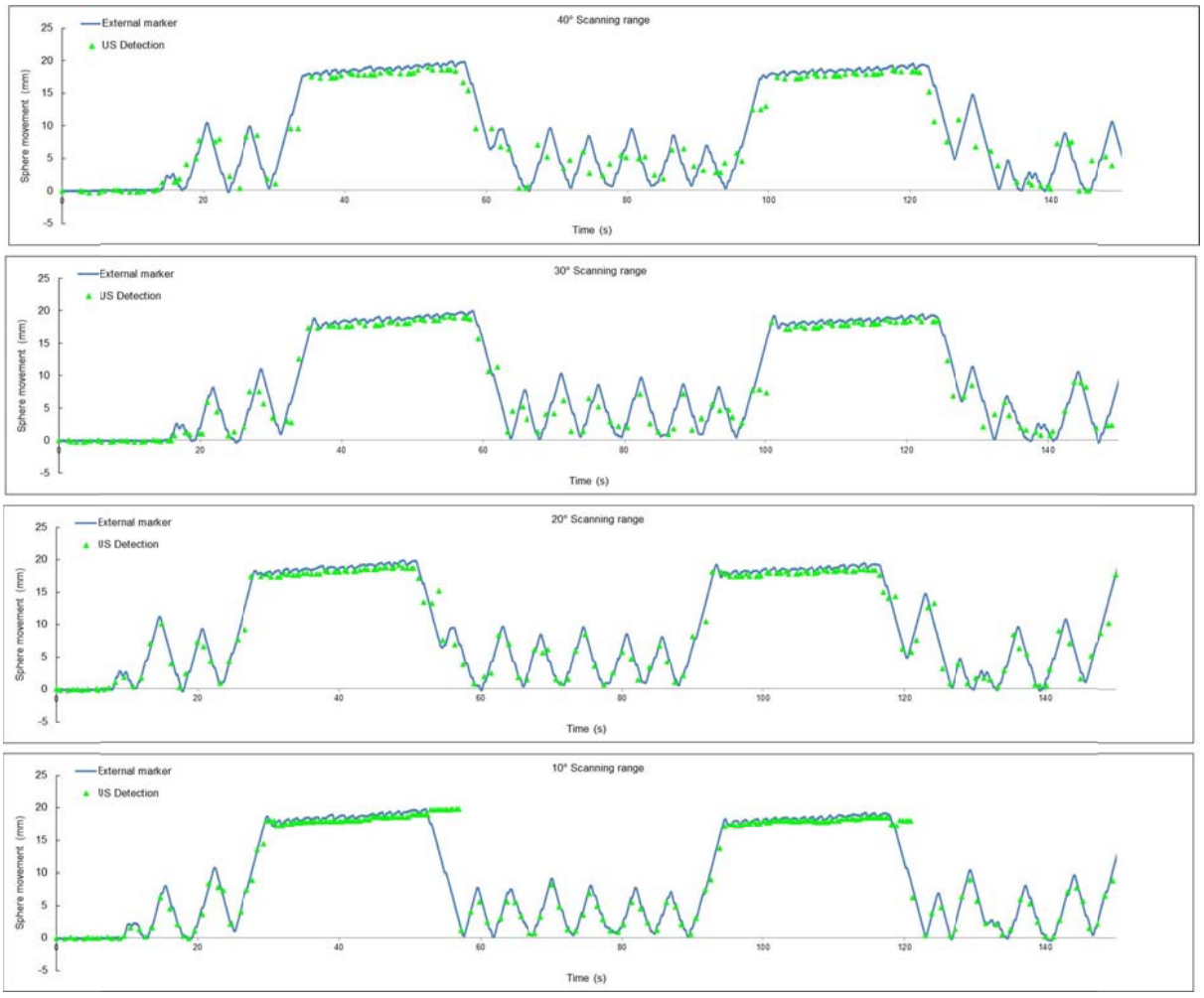

Figure 25. US tracking result of a breathing pattern with various scanning ranges. The accuracy of ultrasound tracking increased with decreasing the scanning range.

Although the accuracy of ultrasound tracking increased with decreasing of the scanning range (increasing scanning frequency), the probability of lost tracking with a small scanning range is higher. Lost tracking occurred when the sweeping range of

the US did not cover whole target. The average amplitude of the free breathing pattern was 11 mm and the maximum amplitude was 15 mm. In the breath-holds phases, the average amplitude was 16 mm and the maximum amplitude was 20 mm. Relevant lost tracking occurred only in the 10° and 20° scanning range for all breathing phases of the emulated cycle. Mean lost tracking incidence occurring at 10° and 20° scanning range was 43.09% and 13.54%, respectively in all phases (breath-hold and spontaneous breathing) of the emulated breathing/breath-hold cycle. It turned out that 30° seemed to be the optimal scanning range at the clinical setting to track along with respiratory motion with a probability of lost tracking below 0.1%.

If the breath-hold phase is separated with free-breathing phase in breathing pattern, the mean differences between the measurement and the reference (mean + position in breath-hold phase is remain constant in all scanning range. While for free-breathing phase, the accuracy of tracking increased with decreasing of the scanning range. The differences between the measurement and the reference position (mean $\pm$ standard deviation) of the sphere motion in breathing pattern, separated between breath-hold phase and free-breathing phase, can be seen in Table 11.

Table 11. The differences between the measurement and the reference position (mean $\pm$ standard deviation) (N=40)) for breathing pattern with separate breath-hold phase and free-breathing phase.

Scanning range (°)	Differences between the measurement and the reference (mean $\pm$ standard deviation) position in mm	
	Breath-hold Phase	Free-breathing Phase
10	0.23 $\pm$ 0.37	0.26 $\pm$ 0.56
20	0.12 $\pm$ 0.22	0.44 $\pm$ 0.71
30	0.14 $\pm$ 0.31	0.83 $\pm$ 1.22
40	0.14 $\pm$ 0.35	0.99 $\pm$ 1.50

3.4 Upper abdominal lesions target monitoring – results of healthy volunteer measurements

The setup of the US probe with the arm-based fixation and combination with computer-controlled DIBH could be applied to all HVs without noticeable inconvenience. This setup was stable during test sessions of about 30 minutes for each HV. Image quality of US-tracking target was sufficient in all cases for definition and tracking/monitoring during DIBH. A representative ultrasound tracking image can be seen in Figure 26a (renal pelvis) and 26b (branches of liver veins).

An example of the tracking curves resulting from ultrasound and surface tracking is shown in Figure 27. A visual check was performed to see whether the target was successfully tracked by the US. US acquisitions that tracked the target successfully resulted in a good correlation between US detection and surface marker (Figure 28).

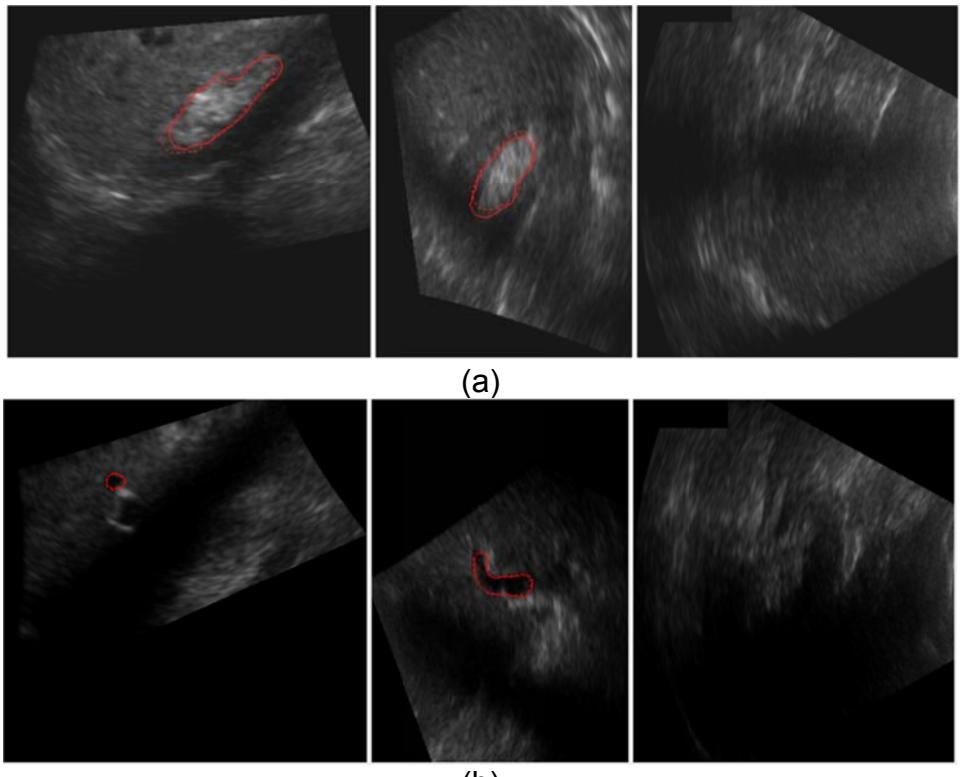

(a)

(b)

Figure 26. Ultrasound tracking of renal pelvis (a) and liver vein branch (b)

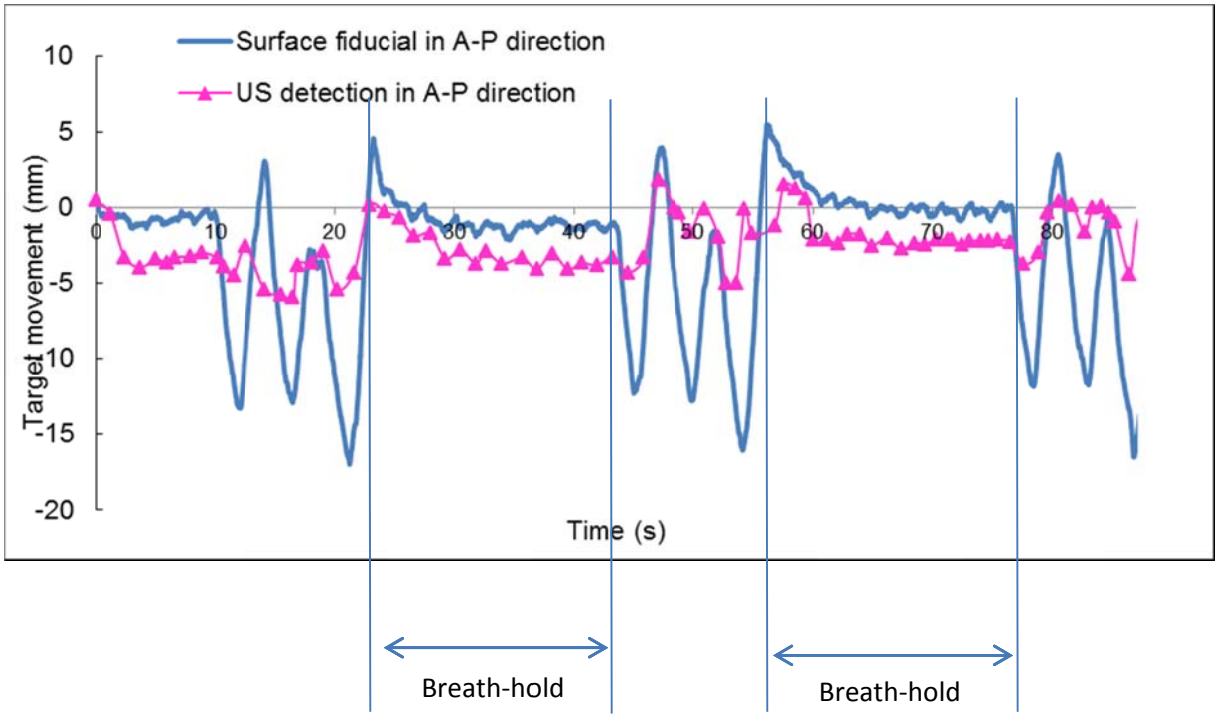

Figure 27. US detection result in AP direction

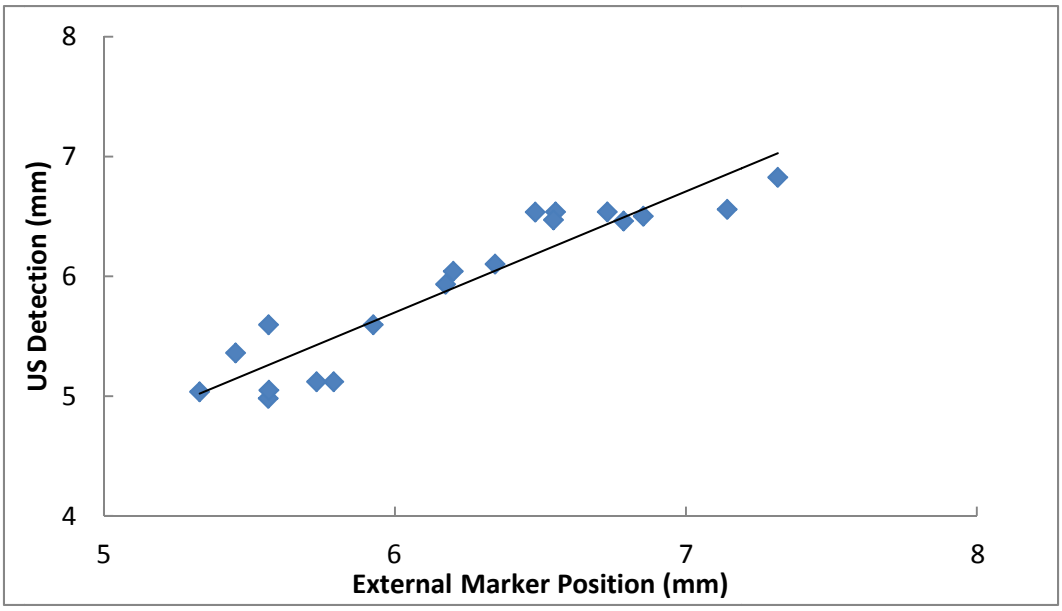

Figure 28. Correlation between displacement of the surface fiducial and tracked structure on US from their respective baselines in 1 breath-hold for good tracking on visual control

There were 74 DIBH phases for renal pelvis and 69 DIBH phases for portal vein branches in total. The success rates of the system to track the target were 93.24% and 89.86% of DIBH phases for renal pelvis and portal vein branches, respectively. US tracking in breath-hold phases correlated well with the surface marker movement

in AP component on the infra-diaphragmatic abdominal wall. Over all HV and scan ranges, the Pearson correlation coefficient (PCC) was strong for most breath-holds analyzed.

Strong correlation (PCC more than 0.71) was observed in 58 (78.38%) and 61 (88.41%) breath-holds in AP and SI direction, respectively for renal pelvis target. Only 9 (12.16%) DIBHs in AP direction and 5 (7.25%) DIBHs in SI direction showed weak correlation (PCC 0.5-0.69). No correlation (PCC less than 0.49) was found in 2 (2.70%) and 3 (4.35%) breath-holds for AP and SI direction, respectively.

For the liver vein target, a strong correlation PCC was found in 51 (73.91%) and 57 (82.61%) breath-holds in AP and SI direction, respectively. Only 6 (8.70%) and 5 (7.25%) breath-holds showed weak correlation PCC in AP and SI direction, respectively. No correlation PCC was found in 5 (7.25%) breath-holds for AP direction. The results can be seen in Table 12.

Scan range and HV did not have a statistically significant effect on the correlation (p values 0.74 and 0.129). For scanning range 40°, a strong correlation PCC was found in 38 and 41 breath-holds in AP and SI direction, respectively. Only 7 and 6 breath-holds showed weak correlation PCC in AP and SI direction, respectively. No correlation PCC was found in 3 and 1 breath-holds in AP and SI direction, respectively. The others scanning range results can be seen in Table 13.

Table 12. The frequency of the Pearson correlation coefficient (PCC) between US tracking and external marker AP movement in breath-hold phase.

Statistical Correlation	**Renal pelvis**		**Portal vein / liver vein branches**	
	AP Direction (n)	SI Direction (n)	AP Direction (n)	SI Direction (n)
Strong PCC (0.70 – 1)	58	61	51	57
Weak PCC (0.50 – 0.69)	9	5	6	5
None PCC (0 – 0.49)	2	3	5	0

Table 13. The frequency of the Pearson correlation coefficient (PCC) between US tracking and external marker movement in breath-hold phase at different scanning range

Statistical Correlation	Renal pelvis		Portal vein / liver vein branches	
	AP Direction (n)	SI Direction (n)	AP Direction (n)	SI Direction (n)
Scanning Range 40°				
Strong PCC (0.70 – 1)	20	23	18	18
Weak PCC (0.50 – 0.69)	4	2	3	4
None PCC (0 – 0.49)	2	1	1	0
Scanning Range 25°				
Strong PCC (0.70 – 1)	21	21	15	19
Weak PCC (0.50 – 0.69)	4	3	2	1
None PCC (0 – 0.49)	0	1	3	0
Scanning Range 10°				
Strong PCC (0.70 – 1)	17	17	18	20
Weak PCC (0.50 – 0.69)	1	0	1	0
None PCC (0 – 0.49)	0	1	1	0

Healthy volunteer no 5 had strong PCC in all breath-holds and both target tracking. Healthy volunteer no 4 had most no correlation PCC and weak correlation with 4 and 14 breath-holds, respectively. The other healthy volunteer results can be seen in Table 14.

Table 14. The frequency of the Pearson correlation coefficient (PCC) between US tracking and external marker movement in breath-hold phase for each healthy volunteer

Statistical Correlation	**Renal pelvis**		**Portal vein / liver vein branches**	
	AP Direction (n)	SI Direction (n)	AP Direction (n)	SI Direction (n)
Healthy Volunteer 1				
Strong PCC (0.70 – 1)	15	15	9	12
Weak PCC (0.50 – 0.69)	0	1	2	0
None PCC (0 – 0.49)	1	0	1	0
Healthy Volunteer 2				
Strong PCC (0.70 – 1)	15	15	12	12
Weak PCC (0.50 – 0.69)	0	0	1	2
None PCC (0 – 0.49)	0	0	1	0
Healthy Volunteer 3				
Strong PCC (0.70 – 1)	12	13	13	14
Weak PCC (0.50 – 0.69)	3	1	0	0
None PCC (0 – 0.49)	0	1	1	0
Healthy Volunteer 4				
Strong PCC (0.70 – 1)	12	16	12	15
Weak PCC (0.50 – 0.69)	6	3	2	3
None PCC (0 – 0.49)	1	1	2	0
Healthy Volunteer 5				
Strong PCC (0.70 – 1)	7	7	7	7
Weak PCC (0.50 – 0.69)	0	0	0	0
None PCC (0 – 0.49)	0	0	0	0

3.5 Upper abdominal target monitoring in patients treated by DIBH-SBRT – intra breath-hold residual motion during CBCT and beam delivery

There were 639 individual DIBHs during 117 CBCT sessions and 509 individual BHs during the beam delivery of 61 treatment sessions that have been analyzed. On visual control of results during CBCT, target was lost in 27.9% of tracking, leaving 490 BHs with optimal tracking in CBCT session. The overall mean(±SD) target displacement during BHs in CBCT session were 1.58(±0.77) mm, 0.77(±0.34) mm, 2.10(±0.86) mm and 3.02(±0.97) mm for SI, LR, AP and 3D vector, respectively. For treatment session, the mean(±SD) target displacement were 1.33(±0.54) mm, 0.71(±0.25) mm, 1.58(±0.62) mm and 2.48(±0.66) mm for SI, LR, AP and 3D vector, respectively.

Most of the target displacements were below 2 mm in CBCT and treatment session as well, with percentage of 69.1%, 90.0%, 62.7% and 42.6% of data for SI, LR, AP and 3D vector, respectively for CBCT session. The complete result of target displacement can be seen in Table 15 and Figure 29. For the treatment session, target displacements below 2 mm were 74.6%, 92.7%, 70.9%, and 49.8% of data for SI, LR, AP and 3D vector, respectively. The complete result of target displacement can be seen in Table 16 and Figure 30.

Table 15. Target displacement in SI, LR, AP and 3D vector (in % of data) during CBCT acquisition in repeated DIBH

Target Displacement (% of data)	SI	LR	AP	3D Vector
< 2 mm	69.1	90.0	62.7	42.6
2 - 5 mm	25.1	9.4	30.0	39.6
5 - 7 mm	4.4	0.5	4.7	10.9
7 - 10 mm	1.2	0.1	2.3	5.8
> 10 mm	0.1	0.0	0.3	1.2

Table 16. Target displacement in SI, LR, AP and 3D vector (in %) at treatment session (during beam delivery)

Target Displacement (% of data)	SI	LR	AP	3D Vector
< 2 mm	74.6	92.7	70.9	49.8
2 - 5 mm	21.4	6.7	24.9	38.3
5 - 7 mm	3.3	0.4	2.9	8.0
7 - 10 mm	0.6	0.1	1.1	3.1
> 10 mm	0.1	0.2	0.1	0.8

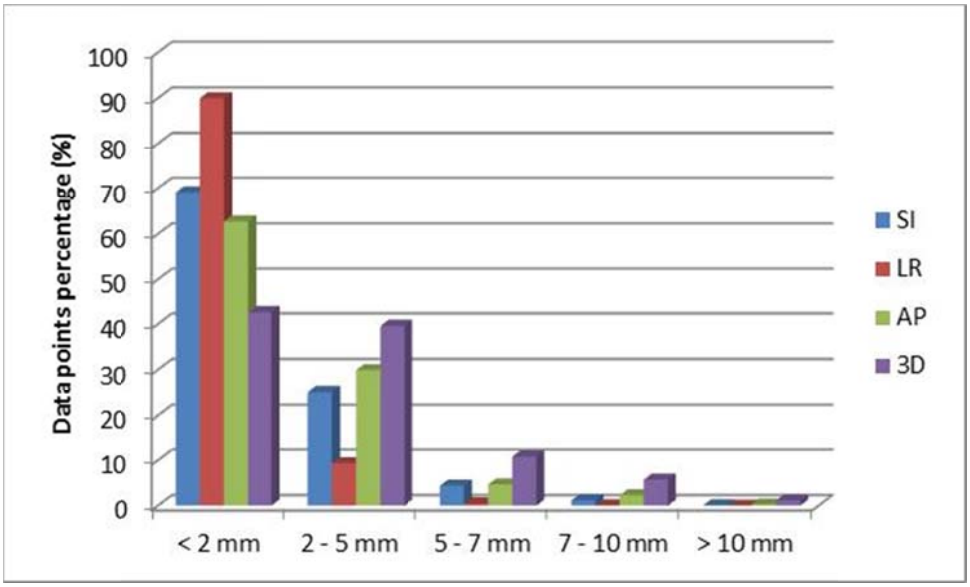

Figure 29. Target displacement in SI, LR, AP and 3D vector (in % of data) for CBCT session

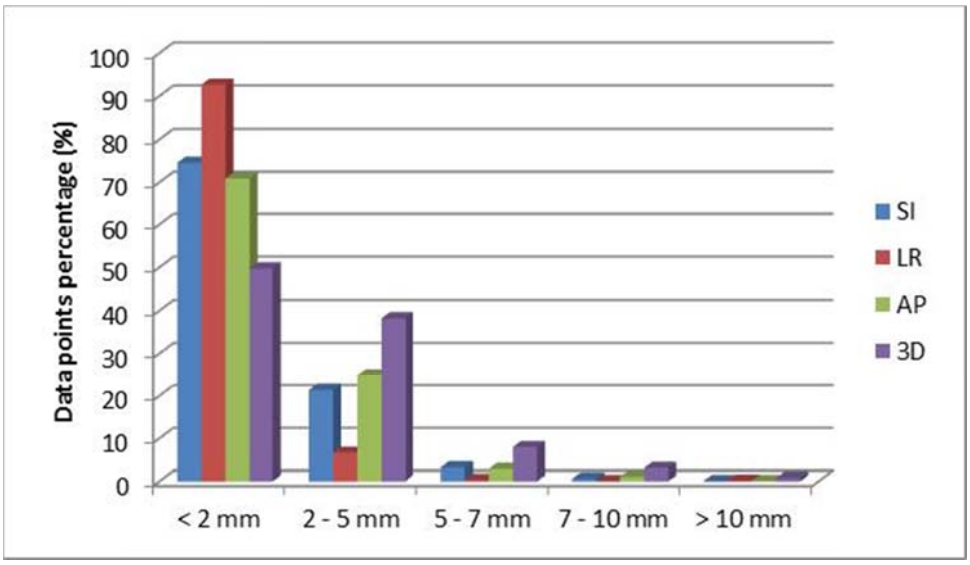

Figure 30. Target displacement in SI, LR, AP and 3D vector (in % of data) at treatment session

The percentage of large target displacement increased with added BH time. At first 5 s, 3D vector of target displacement >10 mm could be observed in 0% of data. Percentage values increased to 0.2%, 0.6%, and 1.2% at 10 s, 15 s and 20 s, respectively in CBCT session. The complete result of target displacement with added BH time in CBCT session can be seen in Table 17 and Figure 31. For treatment session the percentage of large target displacements > 10mm were 0.0%, 0.2%, 0.5% and 0.8% for 5s, 10s, 15s and 20s, respectively. The complete result of target

displacement with added BH time in treatment session can be seen in Table 18 and Figure 32.

Table 17. 3D vector target displacement percentage of added BH duration (in %) at CBCT session

DIBH duration (s)	< 2mm	2-5 mm	5-7 mm	7-10 mm	>10 mm
5	77.9	19.5	1.9	0.6	0.1
10	58.3	33.9	5.2	2.3	0.3
15	47.9	38.6	8.7	4.2	0.7
20	42.5	39.7	10.9	5.8	1.2

Table 18. 3D vector target displacement percentage of added BH duration (in %) at treatment session

DIBH duration (s)	< 2mm	2-5 mm	5-7 mm	7-10 mm	>10 mm
5	83.5	15.5	0.9	0.1	0.1
10	65.3	30.1	3.7	0.6	0.3
15	55.2	35.7	6.4	2.1	0.6
20	50.4	37.7	7.9	3.1	0.8

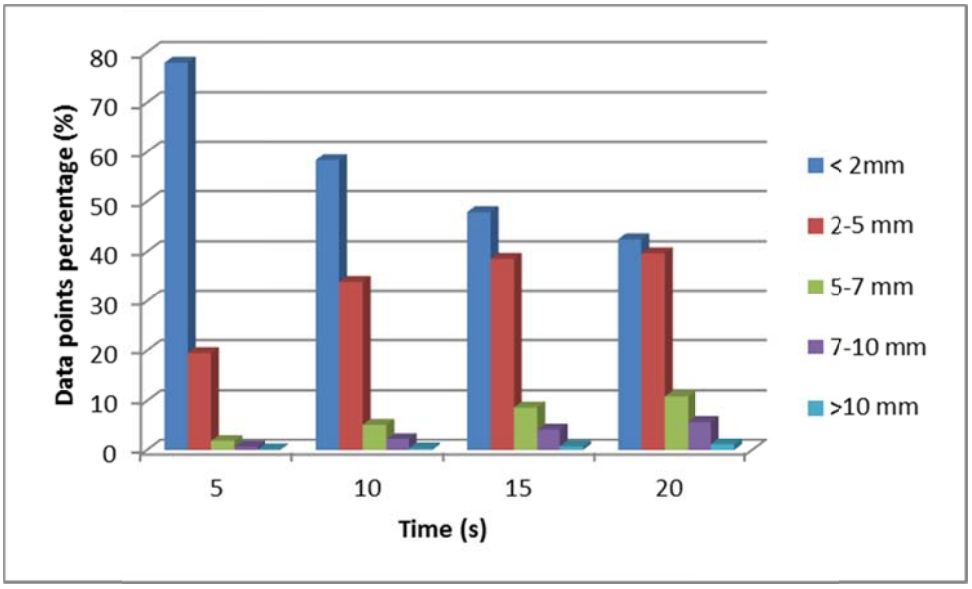

Figure 31. 3D vector target displacement percentage of added BH duration (in %) at CBCT session

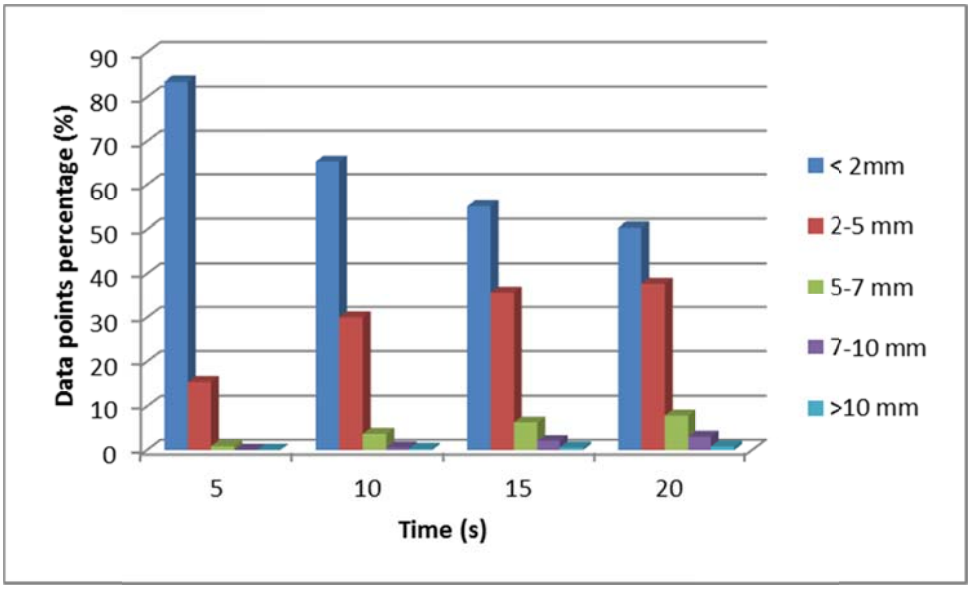

Figure 32. 3D vector target displacement percentage of added BH duration (in %) at treatment session

Intra breath-hold target displacement mean results were less than 2 mm in 80.56% of the data. In CBCT session, there were 3 and 7 patients with more than 2 mm mean target displacement in SI and AP direction, respectively. The mean target displacement during BH for each patient in CBCT session can be seen in Table 19. In treatment session, there were 1 and 3 patients with more than 2 mm mean target displacement in SI and AP direction, respectively. The mean target displacement during BH for each patient in treatment session can be seen in Table 20.

Table 19. Mean target displacement during BH for each patient in CBCT session

Patient	Fraction	BH Count	Mean target displacement (mm)			
			SI Direction	RL Direction	AP Direction	3D Vector
1	15	88	3.11 ± 1.28	1.53 ± 0.66	2.00 ± 1.05	4.17 ± 1.43
2	12	65	1.92 ± 1.36	0.50 ± 0.46	0.60 ± 0.46	2.20 ± 1.36
3	8	26	3.22 ± 1.66	1.34 ± 0.78	4.21 ± 2.17	5.68 ± 2.46
4	3	17	1.14 ± 0.81	1.03 ± 0.68	2.56 ± 1.28	3.22 ± 1.26
5	12	64	1.29 ± 0.76	0.31 ± 0.26	1.53 ± 0.75	2.14 ± 0.96
6	4	29	1.61 ± 1.38	0.57 ± 0.43	2.72 ± 2.06	3.34 ± 2.41
7	5	27	1.12 ± 0.88	0.84 ± 0.47	2.56 ± 1.50	3.09 ± 1.55
8	5	25	0.85 ± 0.70	0.58 ± 0.77	1.77 ± 1.09	2.20 ± 1.36
9	5	21	2.27 ± 2.12	0.70 ± 0.47	1.85 ± 1.32	3.34 ± 2.16
10	8	52	0.82 ± 0.65	0.90 ± 0.75	3.24 ± 1.67	3.60 ± 1.73
11	16	76	1.64 ± 1.11	1.04 ± 0.84	1.53 ± 0.95	2.74 ± 1.37
12	5	23	0.60 ± 0.59	0.71 ± 0.98	1.59 ± 1.56	2.03 ± 1.75
13	5	35	1.55 ± 0.93	0.45 ± 0.36	1.66 ± 0.88	2.43 ± 1.16
14	4	26	1.33 ± 0.88	0.52 ± 0.53	1.56 ± 1.03	2.30 ± 1.25
15	10	65	1.24 ± 0.98	0.55 ± 0.62	2.18 ± 1.82	2.79 ± 1.97

Table 20. Mean target displacement during BH for each patient in treatment session

Patient	Fraction	BH Count	Mean target displacement (mm)								
			SI Direction			RL Direction			AP Direction			3D Vector		
1	11	80	2.55	±	1.41	1.15	±	0.66	1.80	±	1.16	3.60	±	1.45
2	11	87	1.22	±	1.07	0.40	±	0.35	0.64	±	0.66	1.63	±	1.12
4	3	25	1.07	±	0.83	1.02	±	1.23	0.99	±	1.12	2.15	±	1.48
5	11	98	1.67	±	1.22	0.57	±	0.55	2.00	±	1.42	2.86	±	1.74
10	5	47	0.96	±	0.70	0.81	±	0.68	2.61	±	1.51	3.09	±	1.50
12	5	42	0.82	±	0.72	0.66	±	0.60	1.43	±	1.00	1.97	±	1.16
13	5	51	1.60	±	1.08	0.65	±	0.47	2.14	±	1.06	2.95	±	1.29
14	4	35	1.18	±	1.03	0.47	±	0.45	1.47	±	1.25	2.19	±	1.45
15	6	44	0.94	±	0.72	0.64	±	0.61	1.15	±	0.99	1.88	±	1.09

4 DISCUSSION

4.1 System Integrity Quality Assurance

There is a new growing interest in US IGRT developments lately, even though it has been around for several years. The Clarity 3DUS guidance system, a 3D intramodality system, was introduced in 2004.[79] The intramodality approach entails comparison of an US image made treatment stage, with a reference US image, acquired at the time of CT simulation, and therefore compares like with like.

Primarily, the US system itself has to be accurate, and the system has to be fully understood to avoid mistakes and misusage. The system tests based on the standard QA phantom showed that the overall geometric accuracy of the Clarity 3D ultrasound system fulfilled the requirements and were inside the acceptance criteria. The precision of an installation for ultrasound based patient positioning has been evaluated by Ballhausen *et al*. [80] and S. van der Meer *et al*.[79] They reported that the average quality control results for planning-side and treatment-side 3D US together were 0.74 ± 0.57 mm. They found that the Clarity 3DUS guidance system is a robust IGRT device that guides the patient to the correct treatment position.

One of the major concerns for US IGRT is the user variability. Not only is the acquisition of the image for most US systems still performed manually, the images may also be more difficult to interpret than e.g. a CT or MR image. The complete body contour is not visible on an US image, therefore structures may be more difficult to identify on an US image. User experience and training have been shown to improve the consistency and reproducibility of US image interpretation among users.

The accuracy of the prostate monitoring algorithm of Clarity system has been validated by Lachaine *et al*.[69] Their experiment was used an ultrasound phantom on a motion platform with certain motion patterns. The mean and standard deviation of the differences between the measured and reference of their result to be 0.2 $\pm$ 0.4 mm, -0.2 $\pm$ 0.2 mm, and -0.0 $\pm$ 0.2 mm, in the LR, AP, and SI directions, respectively. Our result has good agreement with Lachaine *et al*., which are 0.3 $\pm$ 0.2 mm, 0.2 $\pm$ 0.1 mm and 0.1 $\pm$ 0.1 mm in the LR, AP, and SI directions, respectively. Abramowitz et al.[81] performed a comparison study between the Clarity TPUS autoscan system and the Calypso system (Varian Medical Systems, Palo Alto, CA, USA), the system that utilizes transponders implanted into the prostate for positional tracking. They

designed a motorized phantom combined with a prostate-equivalent structure. They found good agreement between the two systems in tracking the embedded prostate-like sphere.[82]

4.2 Prostate intrafraction motion

Intrafraction prostate motion has been evaluated using various techniques, such as kilovoltage (kV) and megavoltage (MV) imaging of implanted fiducials [83-85], magnetic resonance imaging (MRI) [86, 87], implanted electromagnetic transponders [88, 89], and ultrasound.[90]

Several studies have confirmed that the motion of the prostate is random, sporadic, and patient specific, which makes the prediction of the prostate motion difficult.[91] Even for one patient, the prostate motion can be different form one fraction to another fraction.[18] The intrafractional prostate movements were generally small (< 2 mm) as shown in this study but could be also more than 5 mm for some patients. This result was consistent with other reports.[92, 93]

Prostate displacements were occasional fast drift (e.g., due to muscle contraction), short-term drift (e.g., due to gas passage), continuous drift (e.g., due to rectal/bladder filling), and the combination of various movements. The smallest motion occurred in the LR direction, the AP and SI shifts were often occasional or short-term due to gas passage and sometimes correlated with each other.[93, 94]

The mean values of the prostate displacement indicate the prostate drifts more into the posterior and inferior direction in AP and SI direction, respectively. This phenomenon has been also reported by other researchers.[17, 89, 92] Langen *et al.* reported that long treatment times result in an increasing frequency of large displacements, which was also seen in our study. Shortening the treatment time should therefore be an important objective as more than 5 mm motion has been observed during regular IMRT treatment for some patients.[17, 89, 92]

The feasibility of hypofractionated radiotherapy as new standard of care for external-beam radiotherapy of localized prostate cancer,[50] made it having longer treatment times and thus increase the risk of irradiating a substantial amount of high dose outside the target. Adamson *et al.*[95] reported that for protocols with CBCT guidance in hypofractionated radiotherapy, RL, AP, and SI margins of 2, 4, and 3 mm are sufficient to account for translational errors. However, the large variation in

patient-specific margins suggests that adaptive motion management may be beneficial.[96]

Nevertheless, the systematic error (Σ) and the random error (σ) of intrafraction motion found in this report were small. The systematic errors reported by Litzenberg et al. [97] included setup errors and were larger, with Σ = 0.67 mm, 2.15 mm and 2.62 mm in the LR, AP and SI direction, respectively.

However, due to the very asymmetric distribution of prostate motion probability, fixed margin to compensate for intrafraction motion are not completely suitable to account for accurate motion compensation. At the beginning of fraction, the motion can be over-compensated while at the end of the fraction, the margin could be not sufficient anymore. This emphasizes again the need for online tracking and position correction to take into account intrafraction motion in an optimal manner.[91]

4.3 Upper abdominal target monitoring – phantom study

Daily online interfractional soft tissue imaging has become standard in radiotherapy. Non-invasive US-based IGRT for positioning of upper abdominal lesions has previously been shown to improve positioning accuracy.[19, 98] To enable complete intrafractional control of DIBH treatments, that have several procedural and dosimetric advantages in photon and particle therapy,[22] real-time soft tissue tracking is necessary. Currently most tracking methods available in the clinical routine for this purpose are using implanted fiducials or external/surface based tracking.[99-101]

Usability and accuracy of a real-time 4D US tracking system under DIBH for abdominal targets without invasive placement of fiducials has been evaluated under experimental conditions in this paper. Harris *et al*.[102] have shown that accuracies of greater than 1 mm (similar to our results) can be achieved for 3D sinusoidal motion sequences using incremental 3D speckle tracking of a 4D US system in tissue phantom measurements. Our results are also in the range of what has been reported for other non-ultrasound based tracking approaches. Willoughby *et al.*[88] reported that the Calypso system (based on implanted electromagnetic markers), was 1.5 mm ± 0.9 mm for prostate motion. Shirato *et al.*[103] determined the 3D tracking accuracy of a tracking system based on implanted fiducial markers and fluoroscopy using phantom-based experiments to be 1.5 mm. Given these overall results, ultrasound tracking has the potential to be used in lieu of fluoroscopy tracking measurements to eliminate

invasive marker implantation and costs/side effects associated with fluoroscopic markers and the associated radiation doses to patients.[104]

The limitation of these data is that they have been acquired in the phantom environment with a spherical tracked structure ideal for the tracking algorithm. Tracking robustness might be different in the human body with less clear interfaces and more complex, non-spherical structures suitable for tracking. In a second step we therefore performed an *in-vivo* analysis with healthy volunteers.

4.4 Upper abdominal lesions target monitoring – healthy volunteer

As a crucial element of the process, the probe holder can hold the probe effectively in place for prolonged measurement duration. The probe kept completely steady during measurement but seems to retain a minimal flexibility that will be needed in a clinical application.[71] Online comparison with a gold standard (fiducials) is certainly not possible in volunteers but we could assess the correlation of motion timing and orientation with surface markers as a first plausibility test. Correlation data between external marker and organ motion was comparable with the results reported from Fayad et al [105], that used external marker and 4D CT datasets. They found that the highest correlation coefficients between the motion of external surface areas and internal landmarks such as the diaphragm and mediastinal structures as well as the tumor location landmarks were 0.8 ± 0.18 mm and 0.72 ± 0.12 mm for the abdominal and the thoracic regions, respectively.

Lost tracking occurred due to the target not being covered entirely by the sweeping range, especially at a low scanning range. An optimal trade-off between scanning range and scanning frequency has therefore to be found for each target. In addition, further improvement of the tracking algorithm will improve accuracy along with respiratory motion if using larger scanning angles for detection of high-amplitude motion and non-linear transformations of the tracking target. Nevertheless, the additional use of US surveillance of DIBH treatments would already be possible with manual on-line validation of the plausibility of the tracking.

4.5 Upper abdominal target monitoring - intrafraction motion in breath-hold (patient data)

The residual motion of the tracking target during computer-based DIBH assessed by online US-based tracking has been verified by correlated to offline position

determination of the diaphragm-dome according to a noninvasive approach.[77] The offline kV CBCT data show that US tracking has a strong correlation with the diaphragm motion in most patients.

The results from this study are in line with other reports. Organ motion during inhale breath-hold has been investigated for lung cancer patients; studies have reported motion magnitudes during inhale breath-hold of up to approximately 5.4 mm for the diaphragm and 3.8 mm for lung tumors.[106, 107] Other study reported the pancreatic tumor motion during 30-second inhale breath-hold of up to 11 mm and 8 mm in SI and AP direction, respectively.[108] For institutions using DIBH but no additional monitoring tools, a SI safety margin of 10 mm is sufficient, to compensate for residual motion during BHs.

To reduce further residual errors, faster methods of imaging and delivery are needed. Fast imaging with a combination of kV and MV beam [109, 110] is an accurate method for obtaining 3D CBCT data collection for a single BH. Clinical implementation will accelerate the daily IGRT interface and with that, reduce errors that occur between each BH. In addition to the available fast delivery technique,[111] the acceleration of further treatment delivery is ongoing. In an ideal situation, imaging and delivery will be possible with a total of no more than 3 BH in the future.[77]

5 CONCLUSION

The results of the performed Clarity QA measurement showed an accuracy of maximal 0.5 mm in all phantom and probe combinations which met clinically acceptable range < 1 mm.

The 4D US system offers a non-invasive method for online organ motion monitoring without additional ionizing radiation dose to the patient. On average, the smallest intrafraction prostate motion was in the LR direction (0.01 $\pm$ 0.30 mm) and the largest in AP direction (-0.08 $\pm$ 0.34 mm). The magnitudes of intrafraction prostate motion along the SI and AP directions were comparable, with the mean value of -0.08 mm and 0.05 mm for SI and AP, respectively. There were 84.42% of the 3D vector prostate displacements that were less than 2 mm. However, with increased treatment time, larger 3D vector prostate displacements up to 18.3 mm could be observed. Shortening the treatment time can reduce the intrafraction motion and its effects and US monitoring can help to maximize treatment precision particularly in hypofractionated treatment regimens.

The evaluation of 4D US system for upper abdominal organ monitoring during breath-hold application showed a good performance of tracking accuracy in a 4D motion phantom when tracking a target that moves in accordance to a simulating breathing pattern. A 30°scanning range turned out to be an optimal parameter to track along with respiratory motion considering the accuracy of tracking and the possible loss of the tracked structure. The ultrasound tracking system is also applicable to a clinical setup with the tested hardware solution. The tracking capability of surrogate structures for upper abdominal lesions in DIBH is promising but needs further investigation in a larger cohort of patients. Ultrasound motion data show a strong correlation (Pearson correlation coefficient > 0.7) with surface motion data for 86.64% of individual breath-holds. Further improvement of the tracking algorithm is suggested to improve accuracy along with respiratory motion if using larger scanning angles for detection of high-amplitude motion and non-linear transformations of the tracking target.

The exact quantification of residual motion impact requires an in-depth analysis of time spent at every position, nevertheless mean residual motion during DIBH is low with 80.56% of data were less than 2 mm, predominant in SI and AP direction.

Larger displacements of 3D vector >1cm were only infrequently observed (1.2%), for short periods less than 3 sec. Beam interruption at a predefined threshold could take DIBH treatments close to perfection.

6 BIBLIOGRAPHY

1. Mundt AJ and Roeske JC: *Image-Guided Radiation Therapy: A Clinical Perspective*, People's Medical Publishing House-USA, 2011.

2. Boda-Heggemann J, Köhler FM, Küpper B, Wolff D, Wertz Hor, Mai S, Hesser J, Lohr F and Wenz F: Accuracy of ultrasound-based (BAT) prostate-repositioning: A three dimensional on-line fiducial-based assessment with cone-beam computed tomography. *International Journal of Radiation Oncology Biology Physics,* 70**:** 1247-1255, 2008.

3. Bittner N, Butler WM, Reed JL, Murray BC, Kurko BS, Wallner KE and Merrick GS: Electromagnetic tracking of intrafraction prostate displacement in patients externally immobilized in the prone position. *International Journal of Radiation Oncology Biology Physics,* 77**:** 490-495, 2010.

4. Tome WA, Meeks SL, Orton NP, Bouchet LG and Bova FJ: Commissioning and quality assurance of an optically guided three-dimensional ultrasound target localization system for radiotherapy. *Medical Physics,* 29**:** 1781-1788, 2002.

5. Lagendijk JJW, Raaymakers BW, Raaijmakers AJE, Overweg J, Brown KJ, Kerkhof EM, van der Put RW, Hårdemark B, van Vulpen M and van der Heide UA: MRI/linac integration. *Radiotherapy and Oncology,* 86**:** 25-29, 2008.

6. Lagendijk JJW, Raaymakers BW and van Vulpen M: The Magnetic Resonance Imaging–Linac System. *Seminars in Radiation Oncology,* 24**:** 207-209, 2014.

7. Mutic S and Dempsey JF: The ViewRay System: Magnetic Resonance–Guided and Controlled Radiotherapy. *Seminars in Radiation Oncology,* 24**:** 196-199, 2014.

8. Verellen D, Ridder MD, Linthout N, Tournel K, Soete G and Storme G: Innovations in image-guided radiotherapy. *Nature Reviews Cancer,* 7**:** 949-960, 2007.

9. Dang A, Kupelian PA, Cao M, Agazaryan N and Kishan AU: Image-guided radiotherapy for prostate cancer. *Translational andrology and urology,* 7**:** 308-320, 2018.

10. Boda-Heggemann J, Mennemeyer P, Wertz Hor, Riesenacker N, Küpper B, Lohr F and Wenz F: Accuracy of Ultrasound-Based Image Guidance for Daily Positioning of The Upper Abdomen: An Online Comparison with Cone Beam CT. *Int J Radiat Oncol Biol Phys,* 74**:** 892-897, 2009.

11. Lattanzi J, McNeeley S, Pinover W, Horwitz E, Das I, Schultheiss TE and Hanks GE: A comparison of daily CT localization to a daily US-based system in prostate

cancer. *International Journal of Radiation Oncology Biology Physics,* 43**:** 719–725, 1999.

12. Molloya JA, Chan G, Markovic A, McNeeley S, Pfeiffer D, Salter B and Tome WA: Quality assurance of US-guided external beam radiotherapy for prostate cancer: Report of AAPM Task Group 154. *Medical Physics,* 38**:** 857-871, 2011.

13. Schlosser J, Salisbury K and Hristov D: Online Image-based Monitoring of Soft-tissue Displacements for Radiation Therapy of the Prostate. *International Journal of Radiation Oncology Biology Physics,* 83**:** 1633–1640, 2012.

14. Rathaus V, Richter S, Nissenkorn I and Goldberg E: Transperineal ultrasound examination in the evaluation of prostatic size. *Clinical radiology,* 44**:** 383-385, 1991.

15. Terris MK, Hammerer PG and Nickas ME: Comparison of ultrasound imaging in patients undergoing transperineal and transrectal prostate ultrasound. *Urology,* 52**:** 1070-1072, 1998.

16. Griffiths KA, Ly LP, Jin B, Chan L and Handelsman DJ: Transperineal ultrasound for measurement of prostate volume: validation against transrectal ultrasound. *The Journal of urology,* 178**:** 1375-1379, 2007.

17. Li JS, Jin L, Pollack A, Horwitz EM, Buyyounouski MK, Jr. RAP and Ma C-m: Gains from real-time tracking of prostate motion during external beam radiation therapy. *International Journal of Radiation Oncology, Biology, Physics,* 75**:** 1613-1620, 2009.

18. Sihono DSK, Ehmann M, Heitmann S, von Swietochowski S, Grimm M, Boda-Heggemann J, Lohr F, Wenz F and Wertz H: Determination of Intrafraction Prostate Motion During External Beam Radiation Therapy With a Transperineal 4-Dimensional Ultrasound Real-Time Tracking System. *International Journal of Radiation Oncology • Biology • Physics,* 101**:** 136-143, 2018.

19. Boda-Heggemann J, Walter C, Mai S, Dobler B, Dinter D, Wenz F and Lohr F: Frameless stereotactic radiosurgery of a solitary liver metastasis using active breathing control and stereotactic ultrasound. *Strahlenther Onkol,* 182**:** 216-221, 2006.

20. Boda-Heggemann J, Dinter D, Weiss C, Frauenfeld A, Siebenlist K, Attenberger U, Ottstadt M, Schneider F, Hofheinz R-D, Wenz F and Lohr F: Hypofractionated image-guided breath-hold SABR (Stereotactic Ablative Body Radiotherapy) of liver metastases – clinical results. *Radiat Oncol,* 7, 2012.

21. Wong JW, Sharpe MB, Jaffray DA, Kini VR, Robertson JM, Stromberg JS and Martinez AA: The use of active breathing control (ABC) to reduce margin for breathing motion. *Int J Radiat Oncol Biol Phys,* 44**:** 911-919, 1999.

22. Boda-Heggemann J, Knopf A-C, Simeonova-Chergou A, Wertz H, Stieler F, Jahnke A, Jahnke L, Fleckenstein J, Vogel L, Arns A, Blessing M, Wenz F and Lohr F: Deep Inspiration Breath Hold—Based Radiation Therapy: A Clinical Review. *Int J Radiat Oncol Biol Phys,* 94**:** 478-492, 2016.

23. Abbas H, Chang B and Chen ZJ: Motion management in gastrointestinal cancers. *J Gastrointest Oncol,* 5**:** 223-235, 2014.

24. Nakamura K, Sasaki T, Ohga S, Yoshitake T, Terashima K, Asai K, Matsumoto K, Shioyama Y and Honda H: Recent advances in radiation oncology: intensity-modulated radiotherapy, a clinical perspective. *Int J Clin Oncol,* 19**:** 564-569, 2014.

25. Teh BS, Woo SY and Butler EB: Intensity Modulated Radiation Therapy (IMRT): A New Promising Technology in Radiation Oncology. *The Oncologist,* 4**:** 433-442, 1999.

26. Teoh M, Clark CH, Wood K, Whitaker S and Nisbet A: Volumetric modulated arc therapy: a review of current literature and clinical use in practice. *The British Journal of Radiology,* 84**:** 967-996, 2011.

27. Taylor A and Powell MEB: Intensity-modulated radiotherapy--what is it? *Cancer imaging : the official publication of the International Cancer Imaging Society,* 4**:** 68-73, 2004.

28. Podgorsak EB: *Radiation Physics for Medical Physicists*, Springer 2016.

29. Wang JZ, Li XA, D'Souza WD and Stewart RD: Impact of prolonged fraction delivery times on tumor control: A note of caution for intensity-modulated radiation therapy (IMRT). *International Journal of Radiation Oncology Biology Physics,* 57**:** 543-552, 2003.

30. Bese NS, Hendry J and Jeremic B: Effects of prolongation of overall treatment time due to unplanned interruptions during radiotherapy of different tumor sites and practical methods for compensation. *International Journal of Radiation Oncology Biology Physics,* 68**:** 654-661, 2007.

31. Adams EJ, Convery DJ, Cosgrove VP, McNair HA, Staffurth JN, Vaarkamp J, Nutting CM, Warrington AP, Webb S, Balyckyi J and Dearnaley DP: Clinical implementation of dynamic and step-and-shoot IMRT to treat prostate cancer with

high risk of pelvic lymph node involvement. *Radiotherapy and Oncology,* 70**:** 1-10, 2004.

32. Hall EJ and Wuu C-S: Radiation-induced second cancers: the impact of 3D-CRT and IMRT. *International Journal of Radiation Oncology Biology Physics,* 56**:** 83-88, 2003.

33. Iancu D, Mihaila CN and Trandafir DA: Radiotherapy in Advanced Parotid Tumors. In: *Management of Extended Parotid Tumors.* edited by COSTAN, V.-V., Cham, Springer International Publishing, 2016, pp 217-225.

34. Palmaa DA, Verbakela WFAR, Ottob K and Senana S: New developments in arc radiation therapy: A review. *Cancer Treatment Reviews,* 36**:** 393-399, 2010.

35. Dawson LA and Sharpe MB: Image-guided radiotherapy: rationale, benefits, and limitations. *The Lancet Oncology,* 7**:** 848-858, 2006.

36. Mackie TR, Kapatoes J, Ruchala K, Lu W, Wu C, Olivera G, Forrest L, Tome W, Welsh J, Jeraj R, Harari P, Reckwerdt P, Paliwal B, Ritter M, Keller H, Fowler J and Mehta M: Image guidance for precise conformal radiotherapy. *International Journal of Radiation Oncology Biology Physics,* 56**:** 89-105, 2003.

37. John L. Meyer BDK, J.A. Purdy, R. Timmerman: *IMRT, IGRT, SBRT: Advances in the Treatment Planning and Delivery of Radiotherapy*, Karger Medical and Scientific Publisher, 2007.

38. Schallenkamp JM, Herman MG, Kruse JJ and Pisansky TM: Prostate position relative to pelvic bony anatomy based on intraprostatic gold markers and electronic portal imaging. *Int J Radiat Oncol Biol Phys,* 63**:** 800-811, 2005.

39. Chung PW, Haycocks T, Brown T, Cambridge Z, Kelly V, Alasti H, Jaffray DA and Catton CN: On-line aSi portal imaging of implanted fiducial markers for the reduction of interfraction error during conformal radiotherapy of prostate carcinoma. *Int J Radiat Oncol Biol Phys,* 60**:** 329-334, 2004.

40. Wu J, Haycocks T, Alasti H, Ottewell G, Middlemiss N, Abdolell M, Warde P, Toi A and Catton C: Positioning errors and prostate motion during conformal prostate radiotherapy using on-line isocentre set-up verification and implanted prostate markers. *Radiotherapy and oncology : journal of the European Society for Therapeutic Radiology and Oncology,* 61**:** 127-133, 2001.

41. Briere Tina M, Beddar AS and Gillin Michael T: Evaluation of precalibrated implantable MOSFET radiation dosimeters for megavoltage photon beams. *Medical Physics,* 32**:** 3346-3349, 2005.

42. Dobler B, Mai S, Ross C, Wolff D, Wertz H, Lohr F and Wenz F: Evaluation of Possible Prostate Displacement Induced by Pressure Applied during Transabdominal Ultrasound Image Acquisition. *Strahlentherapie und Onkologie,* 182**:** 240-246, 2006.
43. Guckenberger M, Andratschke N, Alheit H, Holy R, Moustakis C, Nestle U and Sauer O: Definition of stereotactic body radiotherapy. *Strahlentherapie und Onkologie,* 190**:** 26-33, 2014.
44. Benedict SH, Cai J, Libby B, Lovelock M, Schlesinger D, Sheng K and Yang W: SRT and SBRT: Current practices for QA dosimetry and 3D. *Journal of Physics: Conference Series,* 250**:** 012057, 2010.
45. Benedict SH, Yenice KM, Followill D, Galvin JM, Hinson W, Kavanagh B, Keall P, Lovelock M, Meeks S, Papiez L, Purdie T, Sadagopan R, Schell MC, Salter B, Schlesinger DJ, Shiu AS, Solberg T, Song DY, Stieber V, Timmerman R, Tomé WA, Verellen D, Wang L and Yin F-F: Stereotactic body radiation therapy: The report of AAPM Task Group 101. *Medical Physics,* 37**:** 4078-4101, 2010.
46. Galvin JM and Bednarz G: Quality Assurance Procedures for Stereotactic Body Radiation Therapy. *International Journal of Radiation Oncology • Biology • Physics,* 71**:** S122-S125, 2008.
47. Global Burden of Disease Cancer C: Global, regional, and national cancer incidence, mortality, years of life lost, years lived with disability, and disability-adjusted life-years for 32 cancer groups, 1990 to 2015: A systematic analysis for the global burden of disease study. *JAMA Oncology*, 2016.
48. Brenner DJ and Hall EJ: Fractionation and protraction for radiotherapy of prostate carcinoma. *International Journal of Radiation Oncology*Biology*Physics,* 43**:** 1095-1101, 1999.
49. Wolff D, Stieler F, Welzel G, Lorenz F, Abo-Madyan Y, Mai S, Herskind C, Polednik M, Steil V, Wenz F and Lohr F: Volumetric modulated arc therapy (VMAT) vs. serial tomotherapy, step-and-shoot IMRT and 3D-conformal RT for treatment of prostate cancer. *Radiotherapy and Oncology,* 93**:** 226-233, 2009.
50. Dearnaley D, Syndikus I, Mossop H, Khoo V, Birtle A, Bloomfield D, Graham J, Kirkbride P, Logue J, Malik Z, Money-Kyrle J, O'Sullivan JM, Panades M, Parker C, Patterson H, Scrase C, Staffurth J, Stockdale A, Tremlett J, Bidmead M, Mayles H, Naismith O, South C, Gao A, Cruickshank C, Hassan S, Pugh J, Griffin C and Hall E: Conventional versus hypofractionated high-dose intensity-modulated radiotherapy for

prostate cancer: 5-year outcomes of the randomised, non-inferiority, phase 3 CHHiP trial. *The Lancet Oncology,* 17**:** 1047-1060, 2016.

51. Catton CN, Lukka H, Gu CS, Martin JM, Supiot S, Chung PWM, Bauman GS, Bahary JP, Ahmed S, Cheung P, Tai KH, Wu JS, Parliament MB, Tsakiridis T, Corbett TB, Tang C, Dayes IS, Warde P, Craig TK, Julian JA and Levine MN: Randomized Trial of a Hypofractionated Radiation Regimen for the Treatment of Localized Prostate Cancer. *Journal of clinical oncology : official journal of the American Society of Clinical Oncology,* 35**:** 1884-1890, 2017.

52. Arcangeli G, Saracino B, Arcangeli S, Gomellini S, Petrongari MG, Sanguineti G and Strigari L: Moderate Hypofractionation in High-Risk, Organ-Confined Prostate Cancer: Final Results of a Phase III Randomized Trial. *Journal of Clinical Oncology,* 35**:** 1891-1897, 2017.

53. Scorsetti M, Clerici E and Comito T: Stereotactic body radiation therapy for liver metastases. *Journal of Gastrointestinal Oncology,* 5**:** 190-197, 2014.

54. Brandner ED, Chetty IJ, Giaddui TG, Xiao Y and Huq MS: Motion management strategies and technical issues associated with stereotactic body radiotherapy of thoracic and upper abdominal tumors: A review from NRG oncology. *Medical physics,* 44**:** 2595-2612, 2017.

55. Kitamura K, Shirato H, Seppenwoolde Y, Shimizu T, Kodama Y, Endo H, Onimaru R, Oda M, Fujita K, Shimizu S and Miyasaka K: Tumor location, cirrhosis, and surgical history contribute to tumor movement in the liver, as measured during stereotactic irradiation using a real-time tumor-tracking radiotherapy system. *International Journal of Radiation Oncology • Biology • Physics,* 56**:** 221-228, 2003.

56. Balter JM, Ten Haken RK, Lawrence TS, Lam KL and Robertson JM: Uncertainties in CT-based radiation therapy treatment planning associated with patient breathing. *International Journal of Radiation Oncology • Biology • Physics,* 36**:** 167-174, 1996.

57. Smith RP, Bloch P, Harris EE, McDonough J, Sarkar A, Kassaee A, Avery S and Lawrence J. Solin Md: Analysis of interfraction and intrafraction variation during tangential breast irradiation with an electronic portal imaging device. *International Journal of Radiation Oncology Biology Physics,* 62**:** 373-378, 2005.

58. Michalski A, Atyeo J, Cox J and Rinks M: Inter- and intra-fraction motion during radiation therapy to the whole breast in the supine position: A systematic review. *J Med Imaging Radiat Oncol,* 56**:** 499-509, 2012.

59. Litzenberg DW, Balter JM, Hadley SW, Hamstra DA, R.Willoughby T, Kupelian PA, Djemil T, ArulMahadevan, Jani S, Weinstein G, Solberg T, Enke C, Levine L and Sandler HM: Prostate Intrafraction Translation Margins for Real-Time Monitoring and Correction Strategies. *Prostate Cancer,* 2012, 2012.

60. Zhang P, Hunt M, Happersett L, Cox B and Mageras G: Incorporation of treatment plan spatial and temporal dose patterns into a prostate intrafractional motion management strategy. *Medical Physics,* 39**:** 5429-5436, 2012.

61. Bissonnette J-P, Franks KN, Purdie TG, Moseley DJ, jakob Sonke J, Jaffray DA, Dawson LA and Bezjak A: Quantifying interfraction and intrafraction tumor motion in lung stereotactic body radiotherapy using respiration-correlated cone beam computed tomography. *International Journal of Radiation Oncology Biology Physics,* 75**:** 688-695, 2009.

62. Sawant A, Venkat R, Srivastava V, Carlson D, Povzner S, Cattell H and Keall P: Management of three-dimensional intrafraction motion through real-time DMLC tracking. *Medical Physics,* 35**:** 2050–2061, 2008.

63. Keall PJ, Mageras GS, Balter JM, Emery RS, Forster KM, Jiang SB, Kapatoes JM, Kubo HD, Low DA, Murphy MJ, Murray BR, Ramsey CR, van Herk MB, Vedam SS, Wong JW and Yorke E: The management of respiratory motion in radiation oncology; AAPM Report No. 91, Task Group 76. *Medical Physics,* 33**:** 3874–3900, 2006.

64. Mutanga TF, de Boer HCJ, Rajan V, Dirkx MLP, van Os MJH, Incrocci L and Heijmen BJM: Software-controlled, highly automated intrafraction prostate motion correction with intrafraction stereographic targeting: System description and clinical results. *Medical Physics,* 39**:** 1314–1321, 2012.

65. Ghilezan MJ, Jaffray DA, Siewerdsen JH, Herk MV, Shetty A, Sharpe MB, Jafri SZ, Vicini FA, Matter RC, Brabbins DS and Martinez AA: Prostate gland motion assessed with cine-magnetic resonance imaging (cine-MRI). *International Journal of Radiation Oncology Biology Physics,* 62**:** 406–417, 2005.

66. Willoughby TR, Kupelian PA, Pouliot J, Shinohara K, Aubin M, Mack R, Skrumeda LL, Balter JM, Litzenberg DW, Hadley SW, Wei JT and Sandler HM: Target localization and real-time tracking using the Calypso 4D localization system in patients with localized prostate cancer. *International Journal of Radiation Oncology Biology Physics,* 65**:** 528–534, 2006.

67. Kotte ANTJ, Hofman P, Lagendijk JJW, Vulpen MV and Heide UAVD: Intrafraction motion of the prostate during external beam radiation therapy: Analysis of 427 patients with implanted fiducial markers. *International Journal of Radiation Oncology Biology Physics,* 69**:** 419–425, 2007.

68. Litzenberg D, Dawson LA, Sandler H, Sanda MG, McShan DL, Haken RKT, Lam KL, Brock KK and Balter JM: Daily prostate targeting using implanted radiopaque markers. *International Journal of Radiation Oncology Biology Physics,* 52**:** 699–703, 2002.

69. Lachaine M and Falco T: Intrafractional prostate motion management with the Clarity Autoscan system. *Medical Physics International Journal,* 1**:** 72-80, 2013.

70. Herk Mv, Remeijer P and Lebesque JV: Inclusion of geometric uncertainties in treatment plan evaluation. *International Journal of Radiation Oncology, Biology, Physics,* 52**:** 1407-1422, 2002.

71. Sihono DSK, Vogel L, Weiß C, Thölking J, Wenz F, Lohr F, Boda-Heggemann J and Wertz H: A 4D ultrasound real-time tracking system for external beam radiotherapy of upper abdominal lesions under breath-hold. *Strahlentherapie und Onkologie,* 193**:** 213-220, 2017.

72. Boda-Heggemann J, Fleckenstein J, Lohr F, Wertz H, Nachit M, Blessing M, Stsepankou D, Löb I, Küpper B, Kavanagh A, Hansen VN, Brada M, Wenz F and McNair H: Multiple breath-hold CBCT for online image guided radiotherapy of lung tumors: Simulation with a dynamic phantom and first patient data. *Radiother Oncol,* 98**:** 309-316, 2011.

73. Shimizu S, Shirato H, Xo B, Kagei K, Nishioka T, Hashimoto S, Tsuchiya K, Aoyama H and Miyasaka K: Three-dimensional movement of a liver tumor detected by high-speed magnetic resonance imaging. *Radiother Oncol,* 50**:** 367-370, 1999.

74. Park JC, Park SH, Kim JH, Yoon SM, Song SY, Liu Z, Song B, Kauweloa K, Webster MJ, Sandhu A, Mell LK, Jiang SB, Mundt AJ and Song WY: Liver motion during cone beam computed tomography guided stereotactic body radiation therapy. *Med Phys,* 39, 2012.

75. Hallman JL, Mori S, Sharp GC, Lu H-M, Hong TS and Chen GTY: A four-dimensional computed tomography analysis of multiorgan abdominal motion. *Int J Radiat Oncol Biol Phys,* 83**:** 435-441, 2012.

76. Wiles AD, Thompson DG and Frantz DD: Accuracy assessment and interpretation for optical tracking systems. *Medical Imaging 2004.* SPIE, 2004 pp 12.

77. Vogel L, Sihono DSK, Weiss C, Lohr F, Stieler F, Wertz H, von Swietochowski S, Simeonova-Chergou A, Wenz F, Blessing M and Boda-Heggemann J: Intra-breath-hold residual motion of image-guided DIBH liver-SBRT: An estimation by ultrasound-based monitoring correlated with diaphragm position in CBCT. *Radiotherapy and Oncology*, 2018.

78. Boda-Heggemann J, Weiss C, Vogel L, Siebenlist K, Sihono DSK, Wertz H, Jahnke A, Simeonova-Chergou AO, Ehmann M, Wenz F and Lohr F: Ultrasound-Based Real-Time Tracking During Abdominal Stereotactic Body Radiation Therapy: Ultrasound Probe Does Not Influence Plan Quality Significantly. *International Journal of Radiation Oncology • Biology • Physics,* 96**:** E604-E605, 2016.

79. van der Meer S, Bloemen-van Gurp E, Hermans J, Voncken R, Heuvelmans D, Gubbels C, Fontanarosa D, Visser P, Lutgens L, van Gils F and Verhaegen F: Critical assessment of intramodality 3D ultrasound imaging for prostate IGRT compared to fiducial markers. *Med Phys,* 40**:** 071707, 2013.

80. Ballhausen H, Hieber S, Li M, Belka C and Reiner M: Technical Note: Millimeter precision in ultrasound based patient positioning: Experimental quantification of inherent technical limitations. *Medical Physics,* 41**:** 081718-n/a, 2014.

81. Abramowitz MC, Bossart E, Freedman L, Ishkanian A and Pollack A: Noninvasive real-time prostate tracking using a transperineal ultrasound: a clinical trial comparison to rf transponders with visual confirmation. *International Journal of Radiation Oncology, Biology, Physics,* 84**:** S1338, 2012.

82. Baker M and Behrens CF: Prostate displacement during transabdominal ultrasound image-guided radiotherapy assessed by real-time four-dimensional transperineal monitoring. *Acta Oncologica*, 2015.

83. Kotte ANTJ, Hofman P, Lagendijk JJW, Vulpen MV and Heide UAVD: Intrafraction motion of the prostate during external beam radiation therapy: Analysis of 427 patients with implanted fiducial markers. *International Journal of Radiation Oncology, Biology, Physics,* 69**:** 419–425, 2007.

84. Litzenberg D, Dawson LA, Sandler H, Sanda MG, Mcshan DL, Haken RKT, Lam KL, Brock KK and Balter JM: Daily prostate targeting using implanted radiopaque markers. *International Journal of Radiation Oncology, Biology, Physics,* 52**:** 699–703, 2002.

85. Boda-Heggemann J, Köhler FM, Wertz H, Ehmann M, Hermann B, Riesenacker N, Küpper B, Lohr F and Wenz F: Intrafraction motion of the prostate during an IMRT

session: a fiducial-based 3D measurement with Cone-beam CT. *Radiation Oncology,* 3**:** 37, 2008.

86. Ghilezan MJ, Jaffray DA, Siewerdsen JH, Herk MV, Shetty A, Sharpe MB, Jafri SZ, Vicini FA, Matter RC, Brabbins DS and Martinez AA: Prostate gland motion assessed with cine-magnetic resonance imaging (cine-MRI). *International Journal of Radiation Oncology, Biology, Physics,* 62**:** 406–417, 2005.

87. Mah D, Freedman G, Milestone B, Hanlon A, Palacio E, Richardson T, Movsas B, Mitra R, Horwitz E and Hanks GE: Measurement of intrafractional prostate motion using magnetic resonance imaging. *International Journal of Radiation Oncology, Biology, Physics,* 54**:** 568 - 575, 2002.

88. Willoughby TR, Kupelian PA, Pouliot J, Shinohara K, Aubin M, Roach M, Skrumeda LL, Balter JM, Litzenberg DW, Hadley SW, Wei JT and Sandler HM: Target localization and real-time tracking using the Calypso 4D localization system in patients with localized prostate cancer. *International Journal of Radiation Oncology, Biology, Physics,* 65**:** 528–534, 2006.

89. Langen KM, Willoughby TR, Meeks SL, Santhanam A, Cunningham A, Levine L and Kupelian PA: Observations On Real-Time Prostate Gland Motion Using Electromagnetic Tracking. *International Journal of Radiation Oncology, Biology, Physics,* 71**:** 1084 - 1090, 2008.

90. Pinkawa M, Pursch-Lee M, Asadpour B, Gagel B, Piroth MD, Klotz J, Nussen S and Eble MJ: Image-Guided Radiotherapy for Prostate Cancer : Implementation of Ultrasound-Based Prostate Localization for the Analysis of Inter- and Intrafraction Organ Motion. *Strahlentherapie und Onkologie,* 184**:** 679-685, 2008.

91. Ballhausen H, Li M, Hegemann N-S, Ganswindt U and Belka C: Intra-fraction motion of the prostate is a random walk. *Physics in Medicine and Biology,* 60**:** 549 - 563, 2015.

92. Li JS, Lin M-H, Buyyounouski MK, Horwitz EM and Ma C-M: Reduction of prostate intrafractional motion from shortening the treatment time. *Physics in Medicine and Biology,* 58**:** 4921 - 4932, 2013.

93. Tong X, Chen X, Li J, Xu Q, Lin M-H, Chen L, Price RA and Ma C-M: Intrafractional prostate motion during external beam radiotherapy monitored by a real-time target localization system. *Journal of Applied Clinical Medical Physics; Vol 16, No 2 (2015)*, 2015.

94. Xie Y, Djajaputra D, King CR, Hossain S, Ma L and Xing L: Intrafractional motion of the prostate during hypofractionated radiotherapy. *International Journal of Radiation Oncology, Biology, Physics,* 72**:** 236-246, 2008.
95. Adamson J, Wu Q and Yan D: Dosimetric Effect of Intrafraction Motion and Residual Setup Error for Hypofractionated Prostate Intensity-Modulated Radiotherapy With Online Cone Beam Computed Tomography Image Guidance. *International Journal of Radiation Oncology*Biology*Physics,* 80**:** 453-461, 2011.
96. Sihono DSK, Ehmann M, Heitmann S, von Swietochowski S, Grimm M, Boda-Heggemann J, Lohr F, Wenz F and Wertz H: Determination of intrafraction prostate motion during external beam radiotherapy with a transperineal 4D ultrasound real-time tracking system. *International Journal of Radiation Oncology*Biology*Physics*, 2018.
97. Litzenberg DW, Balter JM, Hadley SW, Sandler HM, Willoughby TR, Kupelian PA and Levine L: Influence of intrafraction motion on margins for prostate radiotherapy. *Int J Radiat Oncol Biol Phys,* 65**:** 548-553, 2006.
98. Gurp EB-v, Meer Svd, Hendry J, Buijsen J, Visser P, Fontanarosa D, Lachainey M, Lammering G and Verhaegen F: Active breathing control in combination with ultrasound imaging: A feasibility study of image guidance in stereotactic body radiation therapy of liver lesions. *Int J Radiat Oncol Biol Phys,* 85**:** 1096 - 1102, 2012.
99. Wong VYW, Tung SY, Ng AWY, Li FAS and Leung JOY: Real-time monitoring and control on deep inspiration breath-hold for lung cancer radiotherapy—Combination of ABC and external marker tracking. *Med Phys,* 37**:** 4673-4683, 2010.
100. Tanguturi SK, Lyatskaya Y, Chen Y, Catalano PJ, Chen MH, Yeo WP, Marques A, Truong L, Yeh M, Orlina L, Wong JS, Punglia RS and Bellon JR: Prospective assessment of deep inspiration breath-hold using 3-dimensional surface tracking for irradiation of left-sided breast cancer. *Pract Radiat Oncol,* 5**:** 358-365, 2015.
101. Stieler F, Wenz F, Scherrer D, Bernhardt M and Lohr F: Clinical evaluation of a commercial surface-imaging system for patient positioning in radiotherapy. *Strahlenther Onkol,* 188**:** 1080-1084, 2012.
102. Harris EJ, Miller NR, Bamber JC, Symonds-Tayler JRN and Evans PM: Speckle tracking in a phantom and feature-based tracking in liver in the presence of respiratory motion using 4D ultrasound. *Phys Med Biol,* 55**:** 3363-3380, 2010.
103. Shirato H, Shimizu S, Kunieda T, Kitamura K, Herk MV, Kagei K, Nishioka T, Hashimoto S, Fujita K, Aoyama H, Tsuchiya K, Kudo K and Miyasaka K: Physical

aspects of a real-time tumor-tracking system for gated radiotherapy. *Int J Radiat Oncol Biol Phys,* 48**:** 1187-1195, 2000.

104. Bell MAL, Byram BC, Harris EJ, Evans PM and Bamber JC: In vivo liver tracking with a high volume rate 4D ultrasound scanner and a 2D matrix array probe. *Phys Med Biol,* 57**:** 1359-1374, 2012.

105. Fayad H, Pan T, Clément J-F and Visvikis D: Technical note: Correlation of respiratory motion between external patient surface and internal anatomical landmarks. *Med Phys,* 38, 2011.

106. Kim DJW, Murray BR, Halperin R and Roa WHY: Held-breath self-gating technique for radiotherapy of non–small-cell lung cancer: A feasibility study. *International Journal of Radiation Oncology*Biology*Physics,* 49**:** 43-49, 2001.

107. Barnes EA, Murray BR, Robinson DM, Underwood LJ, Hanson J and Roa WHY: Dosimetric evaluation of lung tumor immobilization using breath hold at deep inspiration. *International Journal of Radiation Oncology*Biology*Physics,* 50**:** 1091-1098, 2001.

108. Lens E, van der Horst A, Versteijne E, Bel A and van Tienhoven G: Considerable pancreatic tumor motion during breath-holding. *Acta Oncologica,* 55**:** 1360-1368, 2016.

109. Arns A, Blessing M, Fleckenstein J, Stsepankou D, Boda-Heggemann J, Hesser J, Lohr F, Wenz F and Wertz H: Phantom-based evaluation of dose exposure of ultrafast combined kV-MV-CBCT towards clinical implementation for IGRT of lung cancer. *PLoS One,* 12**:** e0187710, 2017.

110. Arns A, Blessing M, Fleckenstein J, Stsepankou D, Boda-Heggemann J, Simeonova-Chergou A, Hesser J, Lohr F, Wenz F and Wertz H: Towards clinical implementation of ultrafast combined kV-MV CBCT for IGRT of lung cancer : Evaluation of registration accuracy based on phantom study. *Strahlenther Onkol,* 192**:** 312-321, 2016.

111. Boda-Heggemann J, Mai S, Fleckenstein J, Siebenlist K, Simeonova A, Ehmann M, Steil V, Wenz F, Lohr F and Stieler F: Flattening-filter-free intensity modulated breath-hold image-guided SABR (Stereotactic ABlative Radiotherapy) can be applied in a 15-min treatment slot. *Radiother Oncol,* 109**:** 505-509, 2013.

7 CURRICULUM VITAE

PERSONAL

Name : Dwi Seno Kuncoro Sihono

Address : Mannheimer Str. 62, 68309 Mannheim

Birth Location : Bandung, Jawa Barat, Indonesia

Birth Date : 29 October 1979

Nationality : Indonesian

Status : Married with 3 children

Email : dwi.seno@sci.ui.ac.id

EDUCATION BACKGROUND

- Since April 2013:
  PhD student, Medical Physics, Department of Radiation Oncology,
  University Medical Center Mannheim, University of Heidelberg
- August 2002 – August 2004:
  Master of Science on Medical Physics, University of Indonesia.
  Master Thesis : The Influence of Wedge Filter on Transmission Factor and Percentage Depth Dose for 6 MV and 10 MV X-rays
- August 1997 – December 2001:
  Bachelor of Science on Physics, University of Indonesia.
  Bachelor Thesis: Peak Scatter Factor for 6 MV and 10 MV X-rays
- 1994 – 1997:
  Senior High School, SMU Negeri 1 Depok

COURSE AND TRAINING

- 4 - 8 December 2011
  4th ESTRO SEAROG Course on Advanced Technologies, Singapore
- 13 September – 1 Oktober 2010
  College of Medical Physics, Digital Imaging Science and Technology to Enhance Healthcare in the Developing Country, ICTP, Trieste, Italy
- 25-29 November 2008
  IAEA/RCA Regional Training Course on Medical Physics in Diagnostic Radiology, Manila, Filipina

- 12 – 23 November 2007 :
  ICTP Regional College on Medical Physics, Mumbai, India
- 1 May 2006 – 30 June 2006 :
  IAEA Fellowship, Medical Physics Training Program at Tata Memorial Hospital, Mumbai, India
- 1 December 2004 – 30 September 2005 :
  IAEA Fellowship, Medical Physics Training Program at Westmead Hospital, Sydney, NSW, Australia
- 21 September – 1 October 2004 :
  Training Course on BATAN-JAERI (JTC) On Application of Nuclear Technique in Industry and Environment, Indonesia National Atomic Energy Agency and Japan Atomic Energy Research Institute, BATAN Education and Training Center Jakarta.
- May 2000 – May 2001 :
  Cisco Networking Academy Program, Department of Physics, Universitas Indonesia.
- 1995 - 1998 :
  English Language Course, Basic – Intermediate - Advanced Level, LB-LIA Pangadegan, Jakarta.

WORK EXPERIENCES

- Since 2003 : Lecturer, Department of Physics, Universitas Indonesia.
- 2006 – 2012 : Medical Physicist (Part Time), Radiation Oncology Persahabatan Hospital Jakarta
- 2001 – 2012 : Instructor, Network and System Engineer, Computer and Networking Laboratory, Department of Physics, Universitas Indonesia.

PUBLICATIONS

- Vogel L, **Sihono DSK**, Weiss C, Lohr F, Stieler F, Wertz H, von Swietochowski S, Simeonova-Chergou A, Wenz F, Blessing M, Boda-Heggemann J (2018) Intra-breath-hold residual motion of image-guided DIBH liver-SBRT: An estimation by ultrasound-based monitoring correlated with diaphragm position in CBCT. Radiotherapy and Oncology. doi:https://doi.org/10.1016/j.radonc.2018.07.007
- **Sihono DSK**, Ehmann M, Heitmann S, von Swietochowski S, Grimm M, Boda-Heggemann J, Lohr F, Wenz F, Wertz H (2018) Determination of Intrafraction Prostate Motion During External Beam Radiation Therapy With a Transperineal 4-Dimensional Ultrasound Real-Time Tracking System. International Journal of Radiation Oncology • Biology • Physics 101 (1):136-143. doi:10.1016/j.ijrobp.2018.01.040 [2]
- Sekar Y, Thoelking J, Eckl M, Kalichava I, **Sihono DSK**, Lohr F, Wenz F, Wertz H (2018) Characterization and clinical evaluation of a novel 2D detector array for conventional and flattening filter free (FFF) IMRT pre-treatment verification. Zeitschrift für Medizinische Physik 28 (2):134-141. doi:https://doi.org/10.1016/j.zemedi.2017.08.003 [3]
- **Sihono DSK**, Vogel L, Weiß C, Thölking J, Wenz F, Lohr F, Boda-Heggemann J, Wertz H (2017) A 4D ultrasound real-time tracking system for external beam radiotherapy of upper abdominal lesions under breath-hold. Strahlentherapie und Onkologie*,* 193**:** 213-220. doi:10.1007/s00066-016-1076-7
- Nwankwo O, Mekdash H, **Sihono DSK**, Wenz F, Glatting G (2015) Knowledge-based radiation therapy (KBRT) treatment planning versus planning by experts: validation of a KBRT algorithm for prostate cancer treatment planning. Radiation Oncology 10 (1):111. doi:10.1186/s13014-015-0416-6
- Boda-Heggemann J, Haneder S, Ehmann M, **Sihono DSK**, Wertz H, Mai S, Kegel S, Heitmann S, von Swietochowski S, Lohr F, Wenz F (2015) Stereotactic ultrasound for target volume definition in a patient with prostate cancer and bilateral total hip replacement. Pract Radiat Oncol 5 (3):197-202. doi:10.1016/j.prro.2014.08.008
- Nwankwo O, **Sihono DSK**, Schneider F, Wenz F (2014) A global quality assurance system for personalized radiation therapy treatment planning for the prostate (or other sites). Physics in Medicine and Biology 59 (18):5575

Abstracts at Conferences

2019 DEGRO Annual Meeting

DSK Sihono, L Streb, L Mertens, I Kalish, J Fleckenstein F Lohr, J Boda-Heggemann (2019) Ultrasound-based monitoring and quantification of intrafraction motion during beam delivery of DIBH-liver SBRT

2018 DEGRO Annual Meeting

L Vogel, **DSK Sihono**, C Weiss, F Lohr, F Stieler, H Wertz, S von Swietochowski, A Simeonova-Chergou, F Wenz, M Blessing, J Boda-Heggemann (2018) Intra-fractional Residual Errors in image-guided Liver-SBRT in Breath-Hold: An Assessment based on the Correlation of ultrasound-based Tracking with Siaphragm Position in CBCT, Strahlenther Onkol (2018) (Suppl) 194:S17–S18

L Streb, **DSK Sihono**, L Vogel, F Stieler, M Blessing, H Wertz, F Lohr, I Kalish, von, Swietochowski S., S Tawackoli, A Arns, F Wenz, J Boda-Heggemann (2018) Intra-fractional Residual Errors in image-guided Liver-SBRT in Breath-Hold: Accuracy of Ultrasound-based daily Repositioning for Liver-SBRT in Breath-Hold: A Determination using Marker-and Liver Contour-based Matching in Cone-Beam-CT, Strahlenther Onkol (2018) (Suppl) 194: S189-S190

2017 ASTRO Annual Meeting

Vogel L, **Sihono DSK**, Lohr F, Stieler F, Wertz H, Simeonova-Chergou AO, Blessing M, Wenz F, Boda-Heggemann J (2017) Ultrasound-Based Tracking of Upper Abdominal Targets during Breath-Hold SBRT: Correlation of Ultrasound Data to Surface Position. International Journal of Radiation Oncology*Biology*Physics 99 (2, Supplement):E732.

2017 AAPM Annual Meeting

D Sihono, L Vogel, F Lohr , H Wertz, A Simeonova-Chergou , F Wenz , J Boda-Heggemann (2017) Quantifying Organ Motion During Deep Inspiration Breath-Hold SBRT of Upper Abdominal Targets Using 4D Ultrasound, 2017 AAPM Annual Meeting , Med. Phys. 44 (6), June 2017

Chen X, Nwankwo O, **Sihono DSK**, Wenz F, Glatting G (2017) A Knowledge-Based Radiation Therapy (KBRT) Algorithm for the Treatment-Planning of Simultaneous Integrated Boost (SIB) target Volumes. Medical Physics 44 (6):2734-2735. doi:10.1002/mp.12304

2017 DEGRO Annual Meeting

Vogel L., **Sihono D. S.K**., Lohr F., Stieler F., Wertz H. Simeonova-Chergou A., Blessing M., Wenz F., Boda-Heggemann J. (2017) Ultrasound-based tracking of upper abdominal targets during breath-hold SBRT: correlation of ultrasound data to surface position, Strahlenther Onkol (2017) (Suppl) 193:S1–S194

2016 ASTRO Annual Meeting

1. **Sihono DSK**, Boda-Heggemann J, Vogel L, Thölking J, Lohr F, Wenz F, Wertz H (2016) Development and Evaluation of a New 4-Dimensional Ultrasound Real-Time Tracking System for External Beam Radiation Therapy of Upper Abdominal Lesions Under Breath Hold : A Phantom Study. International Journal of Radiation Oncology • Biology • Physics 96 (2):E608. doi:10.1016/j.ijrobp.2016.06.2152
2. Boda-Heggemann J, Weiß C, Vogel L, Siebenlist K, **Sihono DSK**, Wertz H, Jahnke A, Simeonova-Chergou AO, Ehmann M, Wenz F, Lohr F (2016) Ultrasound-Based Real-Time Tracking During Abdominal Stereotactic Body Radiation Therapy: Ultrasound Probe Does Not Influence Plan Quality Significantly. International Journal of Radiation Oncology • Biology • Physics 96 (2):E604-E605. doi:10.1016/j.ijrobp.2016.06.2144
3. **Sihono DSK**, Weiß C, Vogel L, Kegel S, Thölking J, Wenz F, Wertz H, Lohr F, Boda-Heggemann J (2016) Evaluation of a 4D Ultrasound (US) Real-Time Tracking System for SBRT of Upper Abdominal Lesions in Healthy Volunteers Under Computer-Controlled Breath Hold: A Correlation of Ultrasound and Surface Motion Data. International Journal of Radiation Oncology • Biology • Physics 96 (2):S63. doi:10.1016/j.ijrobp.2016.06.162

2016 DEGRO Annual Meeting

1. Boda-Heggemann J, Weiß C, Vogel L, Siebenlist K, **Sihono DSK**, Wertz H, Jahnke A, Simeonova-Chergou AO, Ehmann M, Wenz F, Lohr F (2016) Ultrasound-based real time tracking during abdominal SBRT: Ultrasound probe does not influence plan quality significantly. Strahlentherapie und Onkologie 192 (1):20. doi:10.1007/s00066-016-0974-z
2. **Sihono DSK**, Boda-Heggemann J, Vogel L, Thölking J, Lohr F, Wenz F, Wertz H (2016) Development and evaluation of a new 4D ultrasound real-time tracking system for external-beam radiotherapy of upper abdominal lesions under breath-hold - a phantom study. Strahlentherapie und Onkologie 192 (1):20. doi:10.1007/s00066-016-0974-z
3. Ehmann M, **Sihono DSK**, Rheinschmidt S, Boda-Heggemann J, Wertz H, Lohr F, Wenz F (2016) Ultraschallbasierte IGRT zur interfraktionellen Positionierung und intrafraktionellem Online-Tracking beim Prostatakarzinom. Strahlentherapie und Onkologie 192 (1):85. doi:10.1007/s00066-016-0974-z
4. Boda-Heggemann J, Vogel L, **Sihono DSK**, Wertz H, Jahnke A, Budjan J, Attenberger U, Simeonova-Chergou AO, Wenz F, Lohr F (2016) Verwendung von Ultraschall bei der Zielvolumendefinition bei Leber-SBRT. Strahlentherapie und Onkologie 192 (1):87. doi:10.1007/s00066-016-0974-z

ESTRO 2016

Sihono DSK, Boda-Heggemann J, Vogel L, Kegel S, Thölking J, Lohr F, Wenz F, Wertz H (2016) EP-1749: Real-time 4D ultrasound tracking of liver and kidney targets for external-beam radiotherapy. Radiotherapy and Oncology 119:S819. doi:10.1016/S0167-8140(16)33000-6

ASTRO 2015

Nwankwo O, Mekdash H, **Sihono DSK**, Wenz F, Glatting G (2015) Comparison of Knowledge Based Radiation Therapy Treatment Plans Against Expert Plans for Prostate VMAT. International Journal of Radiation Oncology • Biology • Physics 93 (3):E582. doi:10.1016/j.ijrobp.2015.07.2034

DEGRO 2015

Nwankwo O, Mekdash H, **Sihono DSK**, Wenz F, Glatting G (2015) Comparison of knowledge-based radiotherapy treatment plans against expert plans. Strahlentherapie und Onkologie 191 (1):S112. doi:10.1007/s00066-015-0847-x

Workshop in Ultrasound Guidance of Radiation Therapy 2015

Dwi Seno Kuncoro Sihono, Michael Ehmann, Stefan Kegel, Sigrun Heitmann, Sandra von Swietochowski, Mario Grimm, Judit Boda-Heggemann, Frank Lohr, Frederik Wenz, Hansjörg Wertz. Determination of intrafraction prostate motion during IMRT with transperineal ultrasound real-time monitoring, Workshop in Ultrasound Guidance of Radiation Therapy organized by the Institute of Cancer Research, Cookham, UK, 2015.

DGMP 2015

O. Nwankwo, H. Mekdash, **D.S.K. Sihono**, F. Wenz, G. Glatting. *Clinical validation of a knowledge based radiation therapy (KBRT) treatment planning algorithm for the prostate*, Abstract Book of DGMP, September 2015, Marburg, Germany, ISBN 978-3-9816508-8-4.

DGMP 2014

D. S. K. Sihono, S. Kegel, H. Wertz, J.-B. Heggemann, F. Lohr, F. Wenz. *System Integrity Quality Assurance for Image Guided Patient Position with 3D Ultrasound in External Beam Radiotherapy (EBRT)*, Abstract Book of Joint Conference of the SSRMP, DGMP, ÖGMP September 2014, Zurich, Germany, ISBN 987-3-9816508-5-3.

DGMP 2013

O. Nwankwo, **D. S. K. Sihono**, F. Schneider, F. Wenz. *A method to predict the achievable normal tissue sparing in radiation therapy*, Abstract Book Deutsche Gesellschaft für Medizinische Physik (DGMP) September 2013, Köln, Germany, ISBN 978-3-9816002-1-6.

8 ACKNOWLEDGEMENT

First and above of all, I praise Allah, the Lord of the Worlds, the Most Beneficent and the Most Merciful, for blessing me this opportunity and granting me the capability to proceed successfully. A doctoral study is one of my academic journey which does not only improve my scientific view but also the way I think and act in the daily life. This thesis owes its existence to the help, support, and inspiration of several persons. Therefore, I would like to express my sincere appreciation and gratitude to all of them.

I gratefully acknowledge my supervisor, Prof. Dr. Frederik Wenz. He provided me the opportunity to work at UMM as a PhD student. I also gratefully acknowledge my co-supervisor, Dr. Hansjörg Wertz. Without his encouragement, thoughtful guidance, and careful supervision, this thesis would never have taken shape. My thanks also go out Medical Physics staff of UMM, most particularly Chief of Medical Physicist Dipl.-Ing. Volker Steil for support and allowing me uses facilities in Department of Radiation Oncology of UMM.

Next, I want to thank PD Dr. med. Dr. rer. nat Judit Boda-Heggemann and Dr. med. Michael Ehmann for their great supports and cooperation in my research using Clarity. I gratefully acknowledge Prof. Dr. Frank Lohr for his huge contribution and discussion in my research. I also want to thank PD Dr. med. Frank Giordano for his help and support. I thank to Clarity research team in Montréal Canada most particularly David Cooper for their support and great help to provide 4D phantom to UMM.

In this occasion, I also thank to my beloved Indonesian friends in Mannheim and Baden Württemberg, for the warm and happiness they share to my family and me. I also acknowledge my colleagues at Department of Physics Universitas Indonesia, for their supports and helps.

I extend my deepest thanks to my beloved wife, Permai Sari Molyana Yusuf, for her love, faithfulness, and of course, her magical dishes. I thank both my boys Afiqah Khairan Kuncoro and Arfan Sihono, and my daughter Aqila Ayu Nayyara for their cheerful and happiness. My special gratitude to my beloved family in Indonesia: my sister Honika and family, my brothers Ato Catur and Tri Haryo, my parents and brother-in-law Mrs. Ichnaini Raras and Aptridio Yusuf.

Finally, I would like to acknowledge Directorate General of Higher Education, Ministry of Research, Technology, and Higher Education of Republic of Indonesia, for granting me with PhD scholarship.